Current Research (2012) Newfoundland and Labrador Department of Natural Resources Geological Survey, Report 12-1, pages 61-84

GEOCHEMISTRY OF THE HOST ROCKS AND TIMING OF GOLD-ELECTRUM MINERALIZATION AT THE VIKING PROPERTY, NEWFOUNDLAND

M. Minnett[1], H. Sandeman[2] and D. Wilton[1]
[1]Department of Earth Sciences, Memorial University of Newfoundland, St. John's, Newfoundland, A1B 4J6
[2]Mineral Deposits Section

ABSTRACT

The Viking gold property, located approximately 10 km south of the community of Pollards Point in White Bay, western Newfoundland, has been intensely explored over the past three years through a rigorous exploration program. This report is the first comprehensive documentation of the host rocks, as well as the style and timing of gold mineralization. Lithogeochemistry and previous U–Pb geochronology demonstrate that the hosts to mineralization/alteration are ca. *1030 Ma Grenvillian A-type anorogenic granitoids,* ca. *615 Ma continental tholeiitic dykes and inclined sheets of the Long Range dyke swarm and, calc-alkaline lamprophyric dykes of unknown affiliation. Mineralization comprises coarse (50 micron) blebby gold and argentiferous electrum, hosted both within quartz veinlets and as inclusions in the sulphide assemblage (pyrite, galena, sphalerite, and chalcopyrite) of these veins. The mineralization is not refractory and has favourable recovery characteristics. Arsenic concentrations are low and arsenopyrite is absent. Substantial hydrothermal alteration proximal to the mineralization is characterized by gains in SiO_2, Al_2O_3, CaO, CO_2 and LOI. The ^{40}Ar–^{39}Ar thermochronology on late-synkinematic biotite porphyroblasts constrains the age of the last peak (*ca. *250°C) dynamometamorphism in the latest Silurian at 419 Ma, whereas sericite from the alteration assemblage yields plateau and pseudo-plateau ages ranging from 409 ± 12 to 377 ± 1.5 Ma. These observations collectively suggest an atypical, silver-bearing, granite-hosted, orogenic gold deposit that was formed in the Early Devonian from auriferous fluids fluxed along the Doucer's Valley fault system.*

INTRODUCTION

Gold mineralization at the Viking property in the White Bay area, western Newfoundland, has been recognized for over 20 years. Much of the exploration history of the property is summarized in Churchill and Voordouw (2006) and Minnett *et al.* (2010). Recent extensive diamond drilling (Ebert, 2008-2011) has resulted in the discovery of a number of new gold occurrences hosted by the Main River Pluton (interpreted as a Grenvillian granitic pluton) situated at the eastern margin of the Long Range Inlier (LRI; Figure 1). The Thor trend is an extensively investigated zone of alteration and mineralization and comprises a 30- to 80-m-wide, roughly planar zone of strong sericite–quartz–pyrite alteration. The Thor trend has an open strike length currently constrained at about 1500 m and the mineralized zone dips to the west and is open at depth. This trend contains numerous high-grade quartz-sulphide veins of which the Thor vein forms an integral part of this study. An independent resource estimate for the gold mineralization (cut-off grade of 0.20 g/t gold) in the Thor trend gave an indicated resource of 98 000 ounces (3 232 000 tonnes at an average grade of 0.95 g/t) and an inferred resource of 45 000 ounces (2 123 000 tonnes at an average grade of 0.66 g/t; Ebert, 2011).

Gold mineralization identified in the greater White Bay area is hosted by potassic-altered Grenvillian granite that has been unconformably juxtaposed against overlying, locally intensely strained, Cambrian sedimentary units. Gold mineralization also occurs in younger Paleozoic cover rocks of the Sops Arm group (Kerr, 2006a, b). Saunders (1991) described three broad styles of mineralization including structurally controlled mesothermal gold–base-metal mineralization (Type 1), stratabound galena mineralization (Type 2), and minor fluorite and molybdenite occurrences in the Gull Lake Intrusive Suite and Devil's Room Granite (Type 3) in the western White Bay area and noted their close spatial relationship with the Doucer's Valley fault system (DVFS). Because the DVFS is constrained to have likely been active as a Taconic thrust surface (Smyth and Schillereff, 1982; Hinchey and Knight, 2011), and also offsets Carboniferous strata, it may have been episodically active for over 150 m.y. This relationship was inferred by Tuach (1987) to indicate that the fault system provided con-

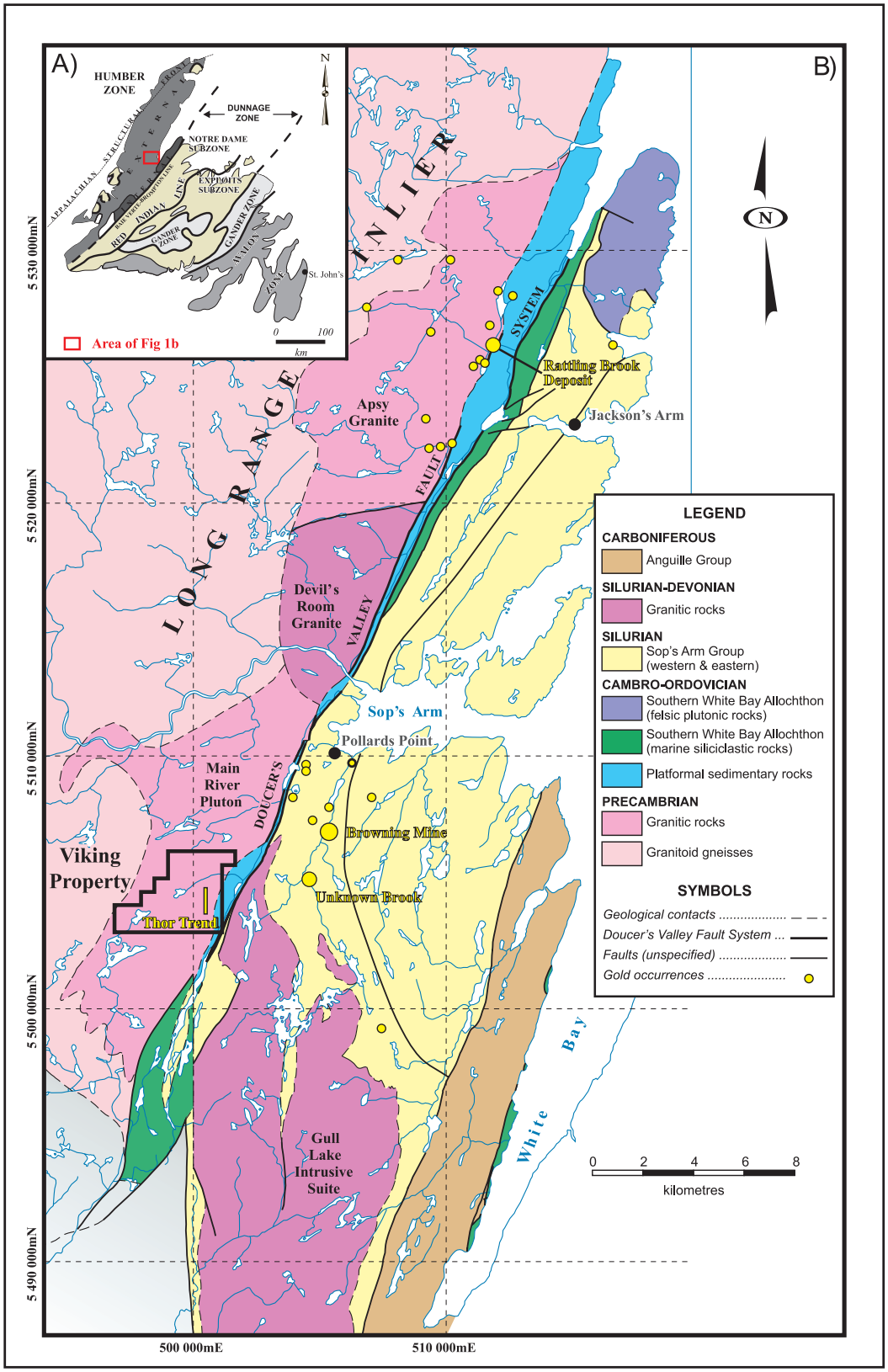

Figure 1. *A) Tectonostratigraphic map of the Island of Newfoundland showing the location of the study area (red box) within the external Humber Zone (Williams, 1995b). B) Simplified regional geology of the White Bay area, western Newfoundland. The Thor trend is highlighted within the Viking property. Modified after Churchill and Voordouw (2006).*

duits for mineralizing hydrothermal fluids on a regional scale and likely over a protracted period of episodic fault movements. This collective system was responsible for precipitating structurally controlled orogenic gold–base-metal mineralization in the volcanic and sedimentary rocks of the Silurian Sops Arm group (*e.g.*, Browning Mine and Unknown Brook; Kerr, 2006a) and in Neoproterozoic granitic rocks and unconformably overlying Cambrian sedimentary rocks (e.g., Rattling Brook and Viking prospects; Kerr, 2005; Minnett *et al.*, 2010). Numerous Grenvillian granitic plutons intruded the LRI at two distinct intervals and their geochemistry and geochronology have been previously studied by Owen (1991) and Heaman *et al.* (2002), respectively. Until this study, whole-rock geochemical data was not available for the Main River Pluton, however, extensive soil and assay sampling has been completed over the area (French, 1987). Recent investigations of the Viking property by Minnett *et al.* (2010) have documented the regional geology and exploration history, and petrography of the host rocks of the deposit.

Based on sparse, robust geochronological evidence, there appears to be a temporal range of gold deposition on the Island of Newfoundland. There is no information on how the timing of gold deposition at the Viking property fits into this temporal range. The ^{40}Ar–^{39}Ar incremental step-heating analysis of pre- and post-mineralization dykes at the Rattling Brook gold deposit constrained the timing of mineralization to the interval *ca.* 415 to 409 Ma, during the latest Silurian or earliest Devonian (Kerr and van Breemen, 2007). Additional geochronological data on the timing of gold mineralization at the Viking property may help to facilitate correlation with other regional, tectonothermal and hydrothermal events.

This study aims to document the stratigraphic and structural controls on alteration and mineralization, the geochemical characteristics of the alteration and host rocks, and the geochronology of alteration and associated gold deposition at the Viking property. Classification of the Viking property gold mineralization will help place it into a regional and temporal context with other examples of gold mineralization in the White Bay area, in other parts of Newfoundland and elsewhere in the Appalachian Orogen.

REGIONAL GEOLOGY

The Paleozoic Appalachian Orogen in Newfoundland records the effects of orogenesis associated with the protracted development and destruction of the Iapetus Ocean (Williams, 1995a). Rocks of the Appalachian Orogen are divided into four broad temporal categories; early Paleozoic and older, middle Paleozoic, late Paleozoic, and Mesozoic. Figure 1A showcases the zonal division of Williams (1976) for the lower Paleozoic and older rocks (from west to east) which are: the Humber, Dunnage, Gander, and Avalon zones (Williams, 1995b). The Humber Zone is separated into external and internal parts based on structural and metamorphic styles (Williams, 1995b). The western margin of the Humber Zone is defined as the limit of Appalachian deformation (*i.e.,* the Appalachian Structural Front) and the eastern margin is drawn at the Baie Verte–Brompton Line. The structural style of the Humber Zone is that of a foreland fold-and-thrust belt, with more deformed and metamorphosed rocks of the internal Humber Zone thrust over the largely undeformed rocks of the external Humber Zone (Williams, 1995b).

The external Humber Zone is subdivided into distinct stratigraphic and structural packages. A polymetamorphosed crystalline basement of the Proterozoic LRI, which is correlated with the Precambrian rocks of the Grenville Province (Canadian Shield) to the northwest, has been intruded by two phases of Grenvillian felsic plutonism (*ca.* 1032–1022 Ma and 993–985 Ma; Heaman *et al.*, 2002) and crosscut by Neoproterozoic Long Range Dykes (615 ± 2 Ma; Kamo *et al.*, 1989). These mafic dykes were emplaced during the initial rifting associated with the opening of the proto-Atlantic ocean (Strong and Williams, 1972; Strong, 1974; Kamo *et al.*, 1989). These basement rocks are unconformably overlain by a series of arkosic clastic units, Cambrian shales and quartzites, and a thick Cambrian to Middle Ordovician carbonate sequence, all of which are capped by a Middle Ordovician shale–sandstone unit. The zone has been affected, with increasing intensity from the Appalachian Structural Front (Figure 1A) eastward, by the Taconic (Middle Ordovician), Salinic (Late Silurian to Early Devonian) and Acadian (Devonian) Orogenic events (Williams, 1995b). The 430.5 ± 2.5 Ma Taylor's Brook Gabbro and the 425 ± 10 Ma Devil's Room Granite are examples of Silurian magmatism within the inlier (Heaman *et al.*, 2002).

STRATIGRAPHIC AND STRUCTURAL CONTROLS ON MINERALIZATION

Mineralization and alteration in the Thor trend are mainly developed in potassium-feldspar megacrystic to augen granodiorite of the Main River Pluton. This porphyritic phase of the pluton has been correlated with the *ca.* 1036 Ma Apsy Granite to the north (Plate 1A, Minnett *et al.*, 2010), which is the host to the Rattling Brook Au prospect (Kerr, 2005). The structural fabrics developed in the megacrystic granodiorite are locally crosscut by metre-scale sheets and sills of variably textured, massive to weakly foliated leucocratic monzogranite. Gabbro–diorite (locally amphibolite) sheets and sills, as well as diabase dykes, are collectively interpreted to be representatives of the Long Range Dyke Swarm that crosscut both the granodiorite and

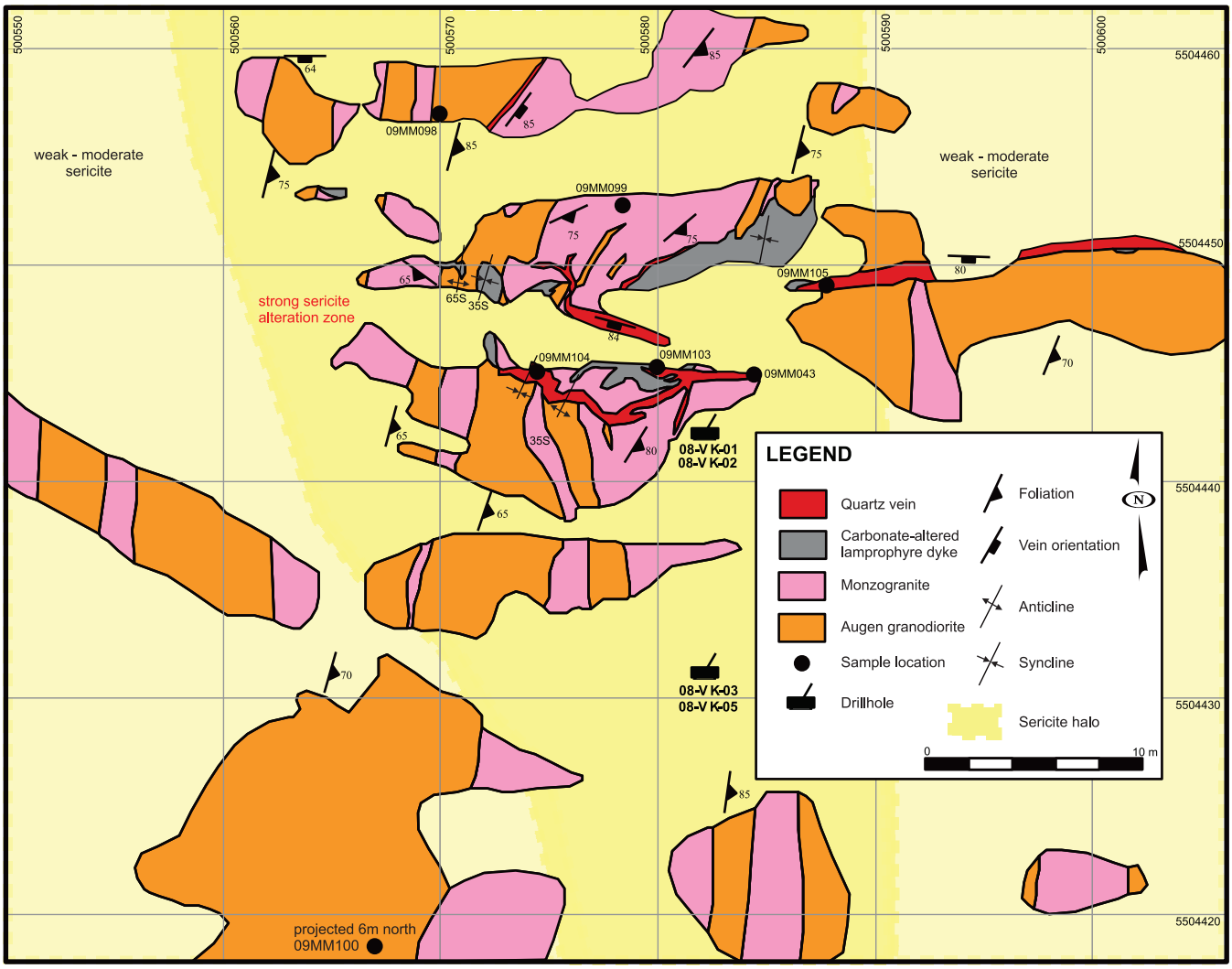

Figure 2. *Simplified geological map of the Thor vein trench exposures. A strongly developed sericitic alteration halo surrounds the east–west-trending vein array that dips to the south.*

the monzogranite. These metamorphosed gabbroic rocks (termed metadykes in subsequent discussion) are typically massive, northeast trending and preserve moderately foliated chilled margins (Plate 3A, Minnett *et al.*, 2010). Similar pre-mineralization metadykes crosscutting the Apsy Granite were dated by ^{40}Ar–^{39}Ar step-heating of metamorphic biotite at 412.3 ± 2.3 Ma (Kerr and van Breemen, 2007). The authors' conclude, however, that this age may represent post-metamorphic cooling, or resetting of metamorphic biotite during alteration related to gold mineralization, and suggested that the dykes were in fact Precambrian. As these dykes were not observed to crosscut rocks of the Labrador Group (*see* below), they therefore may have intruded during the Precambrian and have experienced thermochronological resetting in the latest Silurian to earliest Devonian.

In the vicinity of the Thor vein (Figure 2), fine-grained, locally tightly folded, weakly foliated but strongly carbonate and sericite-altered mesocratic dykes are typically associated with the mineralized veins (Plate 4C *in* Minnett *et al.*, 2010). These dykes are biotite porphyritic and have a matrix of quartz, potassium feldspar, and minor titanite and pyrite. There are no feldspathoid or melilite phenocrysts, or matrix olivine present. The absence of these minerals suggests that these dykes are lamprophyres (Rock, 1991). A robust crystallization age for the mesocratic dykes would provide a maximum age for the Thor mineralization, as brecciated mesocratic dyke fragments are observed in the quartz veins and the dykes are the last evidence of igneous activity in the area.

To the east of the Viking property lie a series of metamorphosed and deformed Cambrian to Ordovician clastic and carbonate rocks interpreted to comprise part of the Labrador Group. Pebble conglomerates of the Bradore Formation are locally observed to preserve a primary uncon-

formable relationship with the Grenvillian basement (Plate 1A). Petrographic examination reveals it is composed of subrounded to rounded, fine- to medium-grained, moderately sorted, weakly deformed quartz clasts in a matrix of fine-grained sericite, weakly chloritized biotite, recrystallized quartz, and pyrite (Plate 1B). Conformable deposition of the Forteau Formation above the Bradore Formation is constrained to the late Early Cambrian (Williams and Stevens, 1969). Both the Bradore and Forteau formations are hydrothermally altered and mineralized adjacent to the Thor trend and, to the north, are juxtaposed against the Apsy Granite, and thus pre-date mineralization.

THOR VEIN MINERALIZATION

Numerous mineralized quartz–sulphide veins of varying thickness have been exposed at surface and intersected in drillcore along the 1500 m length of the Thor trend. The Thor vein is an array of asymmetrical, 30- to 100-cm-thick, openly folded veins having a width of 30 m, at surface (Figure 2). The enveloping surfaces of the veins strike east–west, dip to the south, and continue down dip for at least 100 m. The vertical continuity of the vein array is much greater than the lateral continuity. Numerous narrow shear zones trend perpendicular to the Thor vein and are hosted primarily in the augen granodiorite.

Native gold forms irregular blebs in the quartz–sulphide veins and tiny disseminated grains throughout variably sericite-altered host rocks. Petrographic examination of polished thin sections from the mineralized Thor quartz vein has revealed that gold occurs in two settings: one, as dispersed blebs in the quartz and; two, as micro-inclusions in sulphides that are hosted by quartz. The gold is typically fine grained, forming anhedral, rounded or elongate masses typically less than 50 µm but ranging up to 140 µm in diameter. Gold has locally precipitated along fractures in the quartz vein and in such settings is commonly spatially associated with pyrite and galena. The sulphide assemblage in the veins consists of euhedral, fine- to medium-grained pyrite (2–3%), anhedral, fine-grained sphalerite and galena (1–2%) and lesser amounts of anhedral blebby chalcopyrite (typically ≤ 0.5%). Arsenopyrite was not observed in the Thor vein sections.

Samples from the Thor vein array were selected for scanning electron microscopy (SEM) to verify the presence of Au and its relationships to both sulphide and silicate minerals. Thin sections were cleaned with ethanol, dried, carbon coated, then placed in a mounting stage prior to entering the scanning electron microscope. Backscatter images and element maps were acquired in areas of interest using an acquisition time of 300 seconds. Plate 2 A–C shows that gold clearly occurs as inclusions in pyrite and quartz. As discussed above, gold occurs as inclusions in sphalerite (Plate 2D), and is locally associated with galena. The gold grains are silver-rich and locally occur proximal to examples of what is interpreted to be native silver (Plate 2D). The presence of arsenopyrite was not confirmed in any of the mineralized samples. Fe-rich carbonates (siderite) were considered to be a constituent phase in the alteration assemblage based on field observations (Minnett *et al.*, 2010), yet all of the carbonate minerals observed during SEM analysis were calcite and contained little FeO. Sericite, calcite and pyrite are intergrown with quartz and are spatially and texturally associated with gold grains (Plate 2E). This textural evidence suggests a genetic relationship between the alteration

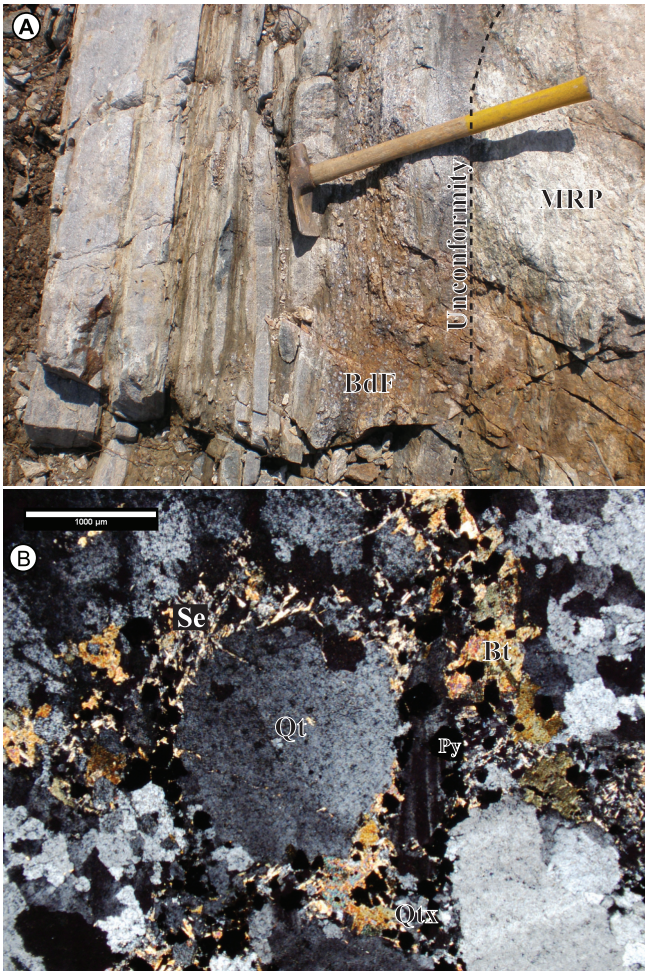

Plate 1. *A) Outcrop photo showing the Main River granodiorite (MRP), to the right, unconformably overlain by Bradore Formation (BdF) sediments to the left. Alteration and conjugate joint sets crosscut the unconformity. Geotul is 1 m in length. B) Photomicrograph of the Bradore Formation pebble conglomerate (cross-polarized light) with rounded quartz clasts (Qt) in a matrix of sericite (Se), biotite (Bt), recrystallized quartz (Qtx), and opaque pyrite (Py).*

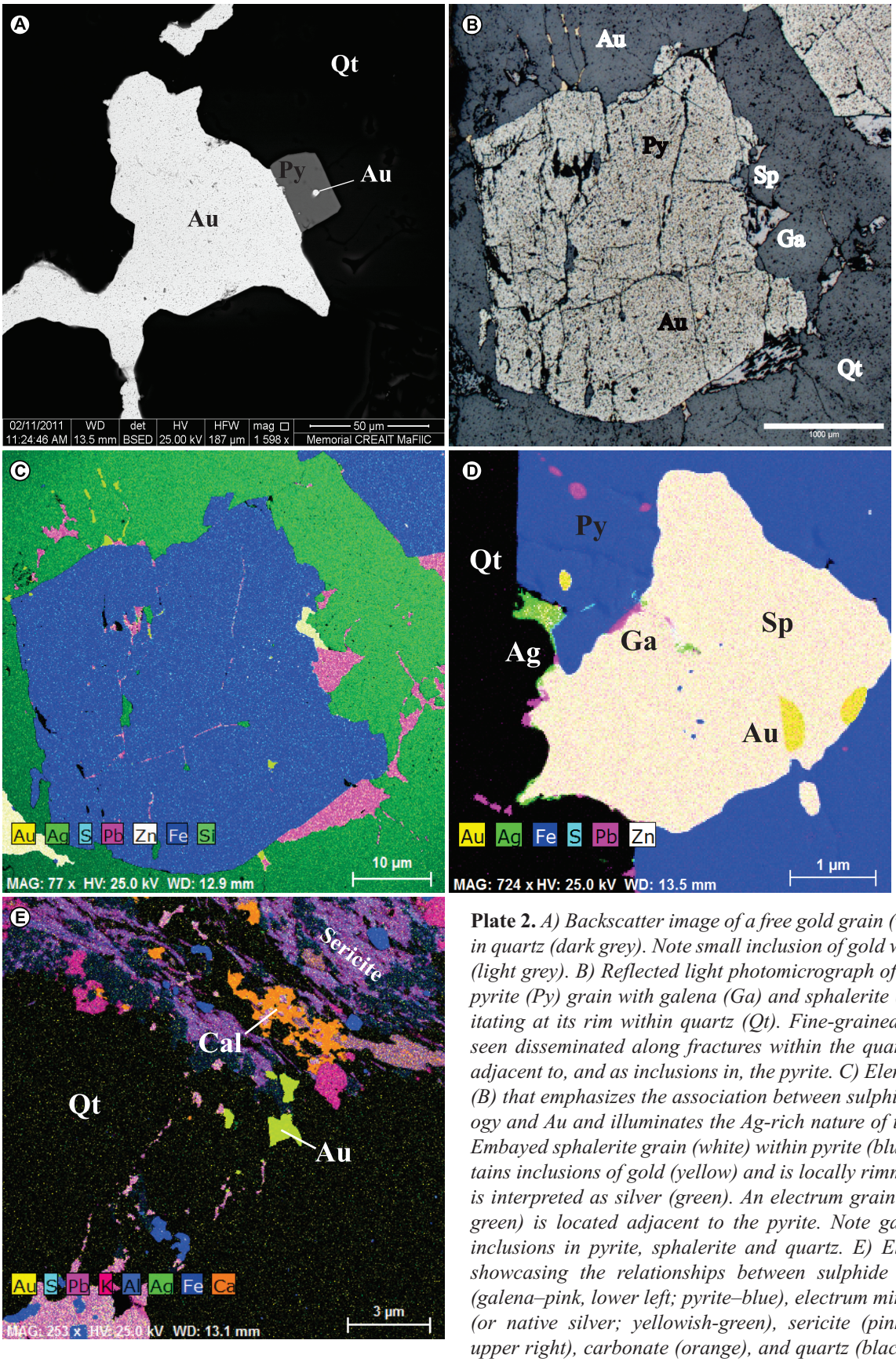

Plate 2. *A) Backscatter image of a free gold grain (white) within quartz (dark grey). Note small inclusion of gold within pyrite (light grey). B) Reflected light photomicrograph of a fractured pyrite (Py) grain with galena (Ga) and sphalerite (Sp) precipitating at its rim within quartz (Qt). Fine-grained Au can be seen disseminated along fractures within the quartz, forming adjacent to, and as inclusions in, the pyrite. C) Element map of (B) that emphasizes the association between sulphide mineralogy and Au and illuminates the Ag-rich nature of the gold. D) Embayed sphalerite grain (white) within pyrite (blue) that contains inclusions of gold (yellow) and is locally rimmed by what is interpreted as silver (green). An electrum grain (yellowish-green) is located adjacent to the pyrite. Note galena (pink) inclusions in pyrite, sphalerite and quartz. E) Element map showcasing the relationships between sulphide mineralogy (galena–pink, lower left; pyrite–blue), electrum mineralization (or native silver; yellowish-green), sericite (pinkish-purple, upper right), carbonate (orange), and quartz (black).*

minerals, gold mineralization, and noted base metal sulphides.

GEOCHEMISTRY

ANALYTICAL METHODS

Host-rock lithogeochemical samples collected during surface traverses and from diamond-drill core include altered host rocks adjacent to, and within, mineralized zones as well as unaltered samples collected remote from mineralization. As such, the whole-rock compositions of many of the host rocks collected as part of this study have been modified by post-crystallization hydrothermal fluid-rock interaction to some extent. Samples of plutons exposed elsewhere in the region were also analyzed for comparison with the rock types of the Main River Pluton. A total of 44 samples were analyzed from both bedrock exposures and drillcore. Minimum, maximum, and average compositions are presented in Table 1.

Major elements were analyzed by ICP-OES at the Geochemical Laboratory of the Department of Natural Resources, Government of Newfoundland and Labrador, following analytical methods described in Finch (1998). Pulverization of the samples was completed using an alumina zirconia swing mill. The samples were also analyzed for high-field-strength elements (HFSE; Y, Zr, Nb, Hf, Ta, and Ga), large-ion-lithophile elements (LILE; Cs, Ba, Rb, Sr, Th, and U), transition elements (V, Cr, Co, Ni), base metals (Cu, Zn, and Pb), volatile elements (Sn, Sb, Tl, and As), and rare-earth elements (REE; La-Lu) by lithium metaborate/tetraborate fusion ICP-MS at Activation Laboratories in Ancaster, Ontario, using the methods documented on their website (http://www.actlabs.com). Gold and Sc were analyzed at Becquerel Laboratories by Neutron Activation Analysis (http://www.becquerellabs.com/).

Assays of mineralized quartz-vein material from the Thor vein were obtained from the Northern Abitibi Mining Corporation database to complement the lithogeochemical samples taken for this study and those results are presented in Table 2. The elements analyzed include Au, Cu, Zn, Pb, As, Ag, Cr, V, Co, Ni, Sn, Sb, W, Ba, Sr, La and Ce. Gold contents were determined by standard fire assay methods at Eastern Analytical, Springdale, Newfoundland, and samples with greater than 5 g/t gold were re-assayed using a metallic sieve procedure to reduce the nugget effect created by free gold particles in the samples.

ELEMENT MOBILITY

Hydrothermal alteration is intense surrounding the mineralized veins at the Viking property, a characteristic common amongst mesothermal lode-gold deposits (Kerrich, 1993; McCuaig and Kerrich, 1998). The mineral assemblages produced during alteration in these deposits are dependent on host rock types, pressure–temperature conditions, and fluid/rock ratios, and typically display enrichments in CO_2, LILE, S, Au and other pathfinder elements (Cassidy *et al.*, 1998). Relative elemental gains and losses were calculated, using the technique from Grant (1986), for the most prominent rock type, the granodiorite, and the results are presented in Figure 3.

Relative gains in the major elements were observed for SiO_2, Al_2O_3, CaO, and LOI. The increase in silica (albeit slight) in the altered samples, is attributed to the inability to remove all of the quartz veinlets from the sample, prior to geochemical analysis. A relative decrease in K_2O, Ba, and Rb may be related simply to the decreased abundance of potassium-feldspar megacrysts in the most altered sample. The concentrations of these elements are expected to increase during the chemical changes brought about during sericitization. A relative increase in CO_2 supports the notion that CO_2-rich fluids are present during alteration and a gain in CaO correlates with the presence of calcite within the alteration assemblage. The base metals, Ag and Au display relative enrichments compared to the least altered sample and pathfinder elements such as Sb, As, W, and Sc are also enriched. Large-ion-lithophile elements display variable depletion with enrichment in Cs and Th and the HFSE and REE appear to be depleted within the alteration halo.

LITHOGEOCHEMISTRY

The rock types of the Viking property have variable major-element chemistry, influenced to a large extent by post-crystallization hydrothermal alteration. The potassium-feldspar megacrystic biotite granodiorite of the Main River Pluton exhibits major-element variations characteristic of calc-alkaline granodiorites, having potassic, granodiorite to granite-like geochemistry (Figure 4A). It has a metaluminous (Figure 4B) composition that is not strongly fractionated and is characterized by intermediate SiO_2 (59.25–70.74 wt.%) and Mg# values (*ca*. 22–35; Table 1). The K_2O content averages 4.42 wt.%, straddling the high-K/shoshonitic boundary on a K_2O–SiO_2 plot (Figure 4C) and they have a modified alkali lime index (MALI; Frost *et al.*, 2001) of approximately 6, suggesting that they are alkalic. The monzogranite sheets that intrude the granodiorites are hypothesized to represent a late-plutonic, significantly more differentiated phase of the pluton, as they have the lowest Mg#'s (average = 30) and highest SiO_2 concentrations. With increasing silica content there is a correlated decrease in Al_2O_3, FeO, MgO, CaO, Na_2O, K_2O, TiO_2, MnO, and P_2O_5. These are dominantly alkali (MALI *ca.* 8) to weakly alkali-calcic, ferroan (Frost *et al.*, 2001), weakly peraluminous,

Table 1. Minimum, maximum and average lithogeochemical compositions for the rock types at the Viking property and the Apsy Granite. All oxides are in weight % and trace elements are in ppm (Au in ppb). $Fe_2O_3^T$- total iron as ferric iron, FeO* - total iron as ferrous iron, Mg# = (molecular MgO/(molecular MgO+FeO^T)), Fe# = FeO*/FeO*+MgO, MALI – modified alkali-lime index 1 (Frost *et al.*, 2001), $_{CN}$ Chondrite Normalized (Sun and McDonough, 1989)

		Main River Granodiorite			Monzogranite			Metadykes			Lamprophyre Dykes			Apsy Granite		
Unit		Minimum	Maximum	Average (n=13)	Minimum	Maximum	Average (n=7)	Minimum	Maximum	Average (n=15)	Minimum	Maximum	Average (n=6)	Minimum	Maximum	Average (n=3)
SiO2	0.02	59.25	70.74	62.91	71.53	75.21	73.62	46.61	55.23	50.01	61.24	63.58	62.36	58.47	72.95	64.33
Al2O3	0.01	10.80	16.65	15.21	13.53	14.47	13.96	11.44	16.48	13.41	14.01	16.19	15.30	13.02	15.55	14.41
Fe2O3	0.01	1.10	2.96	1.99	0.34	0.66	0.53	2.54	7.19	4.83	0.69	2.50	1.53	1.24	3.43	2.36
FeO	0.01	0.38	3.16	2.36	0.01	0.87	0.45	5.05	10.07	8.44	1.65	2.42	2.04	1.33	4.38	2.91
MgO	0.01	0.50	1.72	1.23	0.12	0.53	0.25	3.16	6.70	4.84	1.40	2.05	1.73	0.65	1.89	1.46
CaO	0.01	0.28	4.95	2.96	0.09	0.97	0.45	5.72	10.59	8.24	2.57	3.80	3.41	1.03	4.48	2.68
Na2O	0.01	1.08	4.45	3.75	3.07	4.57	3.70	1.06	4.01	2.79	2.77	4.91	3.64	3.09	3.74	3.41
K2O	0.01	3.43	5.54	4.42	4.44	6.10	5.30	0.38	2.56	1.26	2.96	4.01	3.40	3.28	5.65	4.38
TiO2	0.001	0.59	1.14	0.91	0.06	0.18	0.10	1.73	2.64	2.26	0.54	0.95	0.64	0.33	1.71	1.07
MnO	0.01	0.03	0.09	0.07	0.00	0.02	0.01	0.10	0.33	0.21	0.04	0.06	0.05	0.02	0.14	0.07
P2O5	0.001	0.18	0.38	0.29	0.01	0.05	0.03	0.17	0.65	0.34	0.16	0.31	0.20	0.08	0.63	0.37
LOI	0.01	0.59	5.29	2.64	0.39	1.23	0.77	0.62	2.83	1.32	2.36	6.46	5.00	1.32	1.72	1.49
Total		98.05	99.43	98.75	97.99	99.82	98.88	97.04	99.20	97.95	98.61	100.17	99.31	97.88	100.71	98.94
Fe2O3t	0.01	2.78	5.95	4.61	0.64	1.41	0.97	8.62	16.11	14.21	3.38	5.03	3.79	2.71	8.30	5.60
FeO*	0.01	2.50	5.36	4.15	0.57	1.27	0.92	7.76	14.50	12.79	3.04	4.53	3.41	2.44	7.47	5.04
CO2	0.01	0.02	0.94	0.28	0.02	1.66	0.34	0.01	1.38	0.28	2.43	4.77	3.36	0.09	0.67	0.31
Mg#		22.53	35.78	31.75	22.60	50.16	29.81	31.18	48.03	37.89	33.22	49.52	44.95	28.84	36.20	31.67
Fe#		0.30	0.76	0.64	0.07	0.73	0.55	0.52	0.71	0.63	0.47	0.62	0.54	0.62	0.70	0.66
MALI		1.70	8.37	5.22	7.97	8.93	8.55	-7.81	0.86	-4.20	2.77	5.77	3.64	2.54	7.71	5.11
Sc	0.1	4.60	13.00	8.56	0.60	1.20	0.81	15.00	41.70	34.64	6.50	8.30	7.10	4.30	16.00	11.10
V	5	41.00	64.00	54.69	2.50	7.00	3.79	120.00	449.00	334.80	53.00	62.00	56.33	8.00	69.00	45.00
Cr	20	10.00	10.00	10.00	10.00	10.00	10.00	10.00	130.00	32.00	20.00	30.00	28.33	10.00	10.00	10.00
Co	1	5.00	11.00	7.77	0.50	0.50	0.50	25.00	47.00	38.67	7.00	10.00	8.67	2.00	13.00	8.00
Ni	20	10.00	10.00	10.00	10.00	10.00	10.00	30.00	80.00	44.67	10.00	30.00	20.00	10.00	10.00	10.00
Cu	10	5.00	70.00	27.31	5.00	90.00	18.57	20.00	450.00	237.33	5.00	20.00	11.67	5.00	10.00	6.67
Zn	30	30.00	520.00	158.46	15.00	120.00	32.14	80.00	420.00	153.33	40.00	70.00	55.00	15.00	160.00	91.67
Pb	5	12.00	329.00	66.77	27.00	62.00	39.43	2.50	25.00	10.23	8.00	58.00	20.17	15.00	27.00	21.00
Au	2	1.00	6.00	1.75	1.00	647.00	132.43	1.00	8.00	2.43	1.00	32.00	8.75	1.00	1.00	1.00
Ag	0.5	0.80	3.70	1.68	0.25	0.25	0.25	0.25	1.00	0.34	0.25	0.70	0.38	0.50	1.50	1.03
Sn	1	3.00	7.00	4.46	0.50	8.00	1.57	0.50	4.00	2.00	0.50	2.00	1.08	0.50	2.00	1.50
Sb	0.2	0.10	2.50	0.89	0.10	1.70	0.49	0.10	5.40	0.97	0.10	2.20	1.22	0.10	1.50	0.70
W	0.5	0.25	21.40	7.92	0.25	62.30	11.44	0.25	5.10	1.66	0.70	8.80	3.47	1.00	8.50	4.20
F		237.00	1554.00	1131.85	80.00	375.00	222.71	155.00	1578.00	599.27	452.00	1490.00	847.67	351.21	1154.62	758.30
S	0.01	0.01	0.12	0.07	0.01	0.28	0.09	0.02	0.35	0.10	0.05	0.39	0.16	0.01	0.07	0.03
Tl	0.05	0.71	1.13	0.88	0.50	0.97	0.77	0.07	0.66	0.25	0.37	0.89	0.61	0.49	0.79	0.60
As	5	2.50	120.00	23.46	2.50	32.00	9.71	2.50	12.00	3.13	2.50	21.00	9.08	2.50	2.50	2.50
Cs	0.1	0.40	3.80	1.60	0.10	1.00	0.44	0.05	2.20	0.58	1.40	2.10	1.70	0.40	1.00	0.77
Ba	3	1050.00	2520.00	1844.62	548.00	1790.00	1043.43	62.00	1140.00	384.87	469.00	1300.00	836.00	902.00	1810.00	1454.00
Rb	1	93.00	147.00	121.15	82.00	146.00	121.71	5.00	107.00	32.07	82.00	136.00	110.67	78.00	145.00	105.67
Sr	2	116.00	578.00	410.38	96.00	361.00	181.57	211.00	771.00	333.00	266.00	357.00	322.50	166.00	464.00	304.00
Th	0.05	5.19	19.40	9.98	3.15	14.00	7.88	0.68	3.22	2.14	9.46	10.50	10.12	4.71	9.70	7.15
U	0.01	1.40	3.65	2.30	1.25	17.70	6.45	0.16	0.85	0.63	2.13	2.47	2.29	2.03	3.23	2.67

Y	0.5	36.20	80.20	60.10	3.80	6.10	4.99	28.50	53.60	42.24	9.50	12.10	10.97	33.70	56.00	45.10
Zr	1	390.00	689.00	543.46	48.00	162.00	104.00	123.00	463.00	228.27	176.00	204.00	190.33	330.00	826.00	591.67
Nb	0.2	12.20	31.40	21.55	1.00	4.50	2.19	7.80	35.00	15.15	5.40	6.60	6.20	15.30	32.20	23.17
Hf	0.1	8.70	14.60	11.55	1.50	4.20	2.89	3.00	9.70	5.18	3.90	4.30	4.13	8.20	18.20	13.13
Ta	0.01	1.01	2.65	1.78	0.02	0.13	0.05	0.55	1.49	0.93	0.37	0.44	0.40	0.85	1.84	1.33
Ga	1	20.00	27.00	23.92	16.00	20.00	18.43	18.00	26.00	20.73	19.00	23.00	20.67	20.00	25.00	23.00
Ge	0.5	1.20	2.30	1.65	1.00	1.70	1.21	1.40	2.40	1.78	1.00	2.10	1.32	1.40	1.70	1.53
La	0.05	68.80	127.00	98.56	1.94	37.30	14.39	8.51	70.20	24.57	36.60	44.20	39.75	66.30	87.70	77.93
Ce	0.05	156.00	279.00	224.15	4.51	56.80	24.83	21.20	152.00	54.79	68.90	75.60	72.90	137.00	181.00	158.67
Pr	0.01	19.30	36.70	29.43	0.44	6.59	2.83	3.34	20.00	7.65	7.47	9.11	8.32	17.80	24.50	20.50
Nd	0.05	70.70	137.00	107.95	1.80	21.60	10.01	16.00	77.40	32.51	25.70	31.80	28.83	68.10	95.70	78.17
Sm	0.01	11.30	22.60	17.93	0.52	2.72	1.73	4.28	13.00	7.34	4.01	4.81	4.43	11.50	17.60	13.97
Eu	0.005	1.97	3.78	2.99	0.34	0.95	0.62	1.46	2.97	2.25	1.01	1.23	1.11	1.58	4.18	3.07
Gd	0.01	8.99	19.70	14.72	0.73	2.23	1.50	5.68	10.70	8.73	3.12	3.80	3.48	9.78	16.70	12.89
Tb	0.01	1.23	2.76	2.08	0.11	0.28	0.20	0.87	1.68	1.37	0.37	0.48	0.43	1.40	2.33	1.82
Dy	0.01	6.93	16.00	11.42	0.63	1.39	1.06	5.34	9.99	7.90	1.97	2.35	2.22	7.32	12.00	9.45
Ho	0.01	1.31	2.95	2.15	0.12	0.24	0.19	1.07	1.96	1.54	0.36	0.42	0.39	1.30	2.18	1.71
Er	0.01	3.84	8.52	6.25	0.30	0.65	0.50	3.03	5.60	4.39	1.01	1.13	1.07	3.46	6.00	4.71
Tm	0.005	0.54	1.26	0.90	0.05	0.09	0.07	0.43	0.83	0.63	0.13	0.16	0.15	0.48	0.85	0.66
Yb	0.01	3.25	7.93	5.47	0.33	0.57	0.47	2.76	5.03	3.97	0.82	0.95	0.89	2.88	5.30	4.10
Lu	0.002	0.50	1.16	0.81	0.05	0.08	0.07	0.42	0.78	0.61	0.12	0.14	0.13	0.44	0.81	0.63
(La/Yb)CN		8.97	15.53	13.23	2.44	81.08	26.04	2.21	17.26	4.92	29.60	35.23	31.94	2.45	11.54	5.78
(La/Sm)CN		3.05	4.25	3.59	2.41	9.02	4.99	1.23	4.12	2.00	5.26	6.02	5.80	2.61	11.87	5.90
(Gd/Yb)CN		1.84	2.58	2.24	1.06	5.43	2.87	1.64	2.88	1.86	2.88	3.41	3.22	2.81	19.88	9.05
Au/Ag		0.67	5.45	1.65	4.00	2588.00	529.71	1.00	20.00	7.19	4.00	128.00	35.00	0.67	2.00	1.19

sub-alkaline granites (Figure 4A). The metadykes and gabbroic sheets that crosscut the granitoid rocks are the most primitive, characterized by low SiO_2 (46.61–55.23 wt%) and moderate Mg#'s ranging from 31.2 to 55. They have a wide range of K_2O and exhibit FeO* and TiO_2 enrichment with differentiation. The lamprophyre dykes are strongly sericite and carbonate altered, reflected by enriched CO_2, LOI and K_2O. They qualify as high-K_2O calc-alkaline series rocks based upon the K_2O–SiO_2 diagram of Peccerillo and Taylor (1976). These dykes have Mg#'s that overlap with those of the diabase dykes and sheets, but exhibit intermediate SiO_2, Cr, Ni, Sc, and Co, and high K_2O.

Owing to the variably altered nature of the host rocks, trace elements that are considered to remain immobile during hydrothermal processes are used for further interpretations. The granodiorite has high Ga/Al ratios (*ca.* >2.5) indicating an A-type geochemistry (Figure 5B). Figure 6a shows a custom NMORB-normalized multi-element plot for the granodiorite along with the Apsy Granite and Potato Hill Pluton (Owen *et al.*, 1992). The pattern exhibited by the granodiorite is comparable to those of shoshonitic rocks (*e.g.*, Macdonald *et al.*, 1985; Mauger, 1988; Wyman and Kerrich, 1989) and similar to that of the Apsy Granite and the Potato Hill Pluton. This is underscored by a strong enrichment in LIL elements and LREE [$(La/Sm)_{CN}$ = 3.05-4.25] relative to HREE [$(Gd/Yb)_{CN}$ = 1.84-2.58], Rb and Ba enrichment relative to Sr and Ce and, distinct troughs in the patterns at Ta-Nb, P and Ti. The HFS elements and HREE for the granodiorite and Apsy Granite are generally depleted relative to the Potato Hill Pluton.

The monzogranites have sub-alkaline I-type chemistry (Figure 5B) and have the most depleted REE patterns compared to all other rock types on the Viking property. Rare-earth element abundances decrease with fractionation, a feature that is likely related to fractional crystallization, or separation, of rare-earth-element-bearing accessory phases, such as apatite, monazite or zircon from the residual melt. Akin to the granodiorite, the monzogranite exhibits enrichment in the LILE compared to Sr and Ce and has distinct troughs at Ta–Nb, P and Ti (Figure 6B). The monzogranite sheets exhibit a wide range in LREE enrichment [$(La/Yb)_{CN}$ = 2.44-81.08] with less variable HREE ratios [$(Gd/Yb)_{CN}$ = 1.06-5.43]. Light rare-earth-element concentrations decrease with fractionation, with the most LREE-enriched sample containing the most depleted HREE concentrations. A number of samples show a concave upward REE pattern with a positive Eu anomaly, suggesting feldspar accumulation. The REE patterns for the monzogranite sheets correlate well with the equigranular granite of Owen *et al.* (1992).

The lamprophyre dykes are subalkaline, exhibiting Nb/Y ratios less than 0.8 (Pearce, 1996). They have compo-

Table 2. Assay results for 14 diamond-drill hole samples from the Thor vein. See text for discussion. Au concentration is given in parts per billion (ppb) and the remaining elements are reported in parts per million (ppm). UTM coordinates given in NAD27, Zone 21 format and represent the collar locations from diamond-drill holes and not their surface projections. DL denotes the detection limit for the given element

Sample		**91254**	**91255**	**91256**	**91258**	**91260**	**91261**	**92308**	**92311**	**92312**	**91353**	**91359**	**91361**	**91383**	**58252**
Drill Hole		**08-VK-01**	**08-VK-01**	**08-VK-01**	**08-VK-01**	**08-VK-01**	**08-VK-01**	**08-VK-02**	**08-VK-02**	**08-VK-02**	**08-VK-03**	**08-VK-03**	**08-VK-03**	**08-VK-04**	**08-VK-05**
From (m)		**3.60**	**4.10**	**4.60**	**5.10**	**6.20**	**6.70**	**7.00**	**8.80**	**9.30**	**9.95**	**15.00**	**17.10**	**5.00**	**25.78**
To (m)		**4.10**	**4.60**	**5.10**	**5.40**	**6.70**	**7.70**	**7.40**	**9.30**	**9.80**	**10.45**	**15.50**	**17.40**	**5.39**	**26.70**
Easting		**500582**	**500582**	**500582**	**500582**	**500582**	**500582**	**500582**	**500582**	**500582**	**500582**	**500582**	**500582**	**500651**	**500582**
Northing	**DL**	**5504442**	**5504442**	**5504442**	**5504442**	**5504442**	**5504442**	**5504442**	**5504442**	**5504442**	**5504431**	**5504431**	**5504431**	**5504651**	**5504431**
Au	**5**	222950	44438	41606	6523	79525	1829	42438	856	60331	589	161025	29100	13303	96575
Cu	**1**	114	7	25	11	187	20	91	7	117	4	477	48	34	595
Zn	**1**	1360	392	284	73	1855	85	1576	117	880	212	4000	1112	158	2600
Pb	**2**	3800	835	940	129	2700	94	2024	133	1859	315	2900	2300	134	5500
As	**1**	154	45	26	44	61	23	59	16	27	26	66	43	30	27
Ag	**0.2**	55.1	5.1	4.5	1.1	24.7	0.6	13	0.9	15.4	0.9	11.1	45.7	1.5	43
Cr	**10**	288	318	318	353	318	180	226	223	275	270	265	206	240	230
V	**1**	2	1	1	1	1	1	1	1	1	1	3	3	2	2
Co	**1**	3	2	1	1	3	2	2	1	1	3	4	5	2	3
Ni	**1**	6	5	4	5	7	3	6	4	5	5	8	11	6	6
Sn	**10**	10	10	10	10	10	10	10	10	10	10	10	10	10	10
Sb	**6**	5	5	5	5	5	5	5	5	5	5	5	5	5	5
W	**10**	10	10	10	10	10	10	10	10	10	10	10	10	10	10
Ba	**10**	10	10	10	15	10	32	11	10	10	12	12	17	14	11
Sr	**1**	5	1	2	3	2	9	4	2	3	5	12	35	8	5
La	**10**	10	10	10	10	10	10	10	10	10	10	10	10	13	10
Ce	**10**	22	10	14	20	37	40	24	10	30	18	126	119	43	59
Au/Ag	**n/a**	4	9	9	6	3	3	3	1	4	1	15	1	9	2

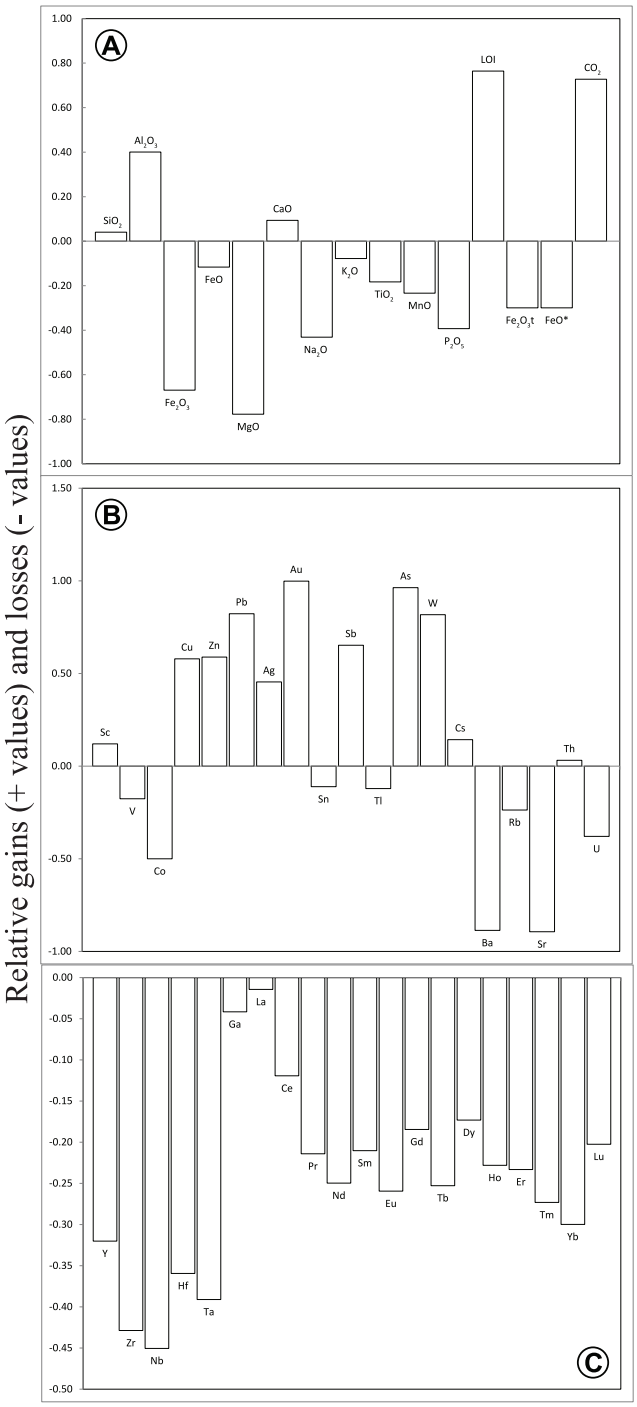

Figure 3. *Relative loss and gains in the Main River granodiorite during hydrothermal alteration at the Viking property. A) Major elements and CO_2, B) transition elements, base metals, mineralization, and LILE, C) HFSE and REE.*

sitions similar to calc-alkaline lamprophyres, characterized by low Nb/Pb and high V/Cr ratios on the immobile trace-element plot of Rock (1991; Figure 5C). Lamprophyres typically exhibit H_2O, CO_2, F, Cl, LILE, P, Rb, Ba, LREE and Th concentrations at levels, 2 to 3 orders of magnitude higher than MORB, but MORB-like levels of Y, Ti, HREE, and Sc (Rock, 1991). Well-developed troughs for Ta, Nb, P and Ti relative to adjacent elements provides evidence that these rocks have geochemical characteristics similar to calc-alkaline lamprophyres of Rock (1991). They show a strong enrichment in the more incompatible elements showcased by elevated Rb, Ba, Th and LREE relative to HFSE and the HREE. They display strong LREE-enriched [$(La/Sm)_{CN}$ = 2.01-6.02] negatively sloped patterns.

The metadykes contain substantial Cr (30–130 ppm) and Ni (30–80 ppm) and are classified as subalkaline and tholeiitic based on their mobile major-element and immobile trace-element chemistry (Irvine and Baragar, 1971; Winchester and Floyd, 1977; Pearce, 1996). The metadykes have the most distinct and varying multi-element plots of the rock types studied. There are four types of dykes that can be distinguished by their LREE, Nb, and HFSE abundances (Figure 6C). Type 1 metadykes have consistent, mutually parallel patterns with a shallow negative slope indicating only slight LREE enrichment relative to the HREE. A second variety (Type 2; n=2) have more fractionated patterns with significant LREE enrichment relative to Th and Nb. This type also shows a distinct negative Ti anomaly and depleted HREE abundances relative to Type 1 and 3 metadykes. Type 3 metadykes (n=1) have a similar pattern to Type 2, however, showcase a positive Nb anomaly. Type 4 metadykes (n=1) have depleted LREE compared to the other types and have a weakly negative sloped pattern with depleted HREE.

ASSAY RESULTS

Fourteen analyses of gold-bearing quartz–sulphide veins from the Thor vein array were added from the Northern Abitibi Mining Corporation assay database to complement the lithogeochemical dataset presented in this study. Gold values range from 589 to 222 950 ppb with higher assay results ascribed to the 'nugget effect' of gold in such deposits containing coarse-grained gold. Gold concentrations correlate with those for the base metals (Cu, Zn, Pb), as well as Ag and As. The relationship observed between base-metal and gold concentrations and the presence of the documented sulphide minerals, suggests that gold should also correlate with sulphur. Gold-bearing veins exhibit variable enrichments in Cu, Zn, and Pb that are elevated significantly above regional background values. The Au/Ag ratios range from 0.6 to 14 (average = 5; Table 2) indicating that Au is enriched relative to Ag. These ratios are generally greater than 5/1 (Au/Ag) for orogenic gold systems (Groves *et al.*, 2003).

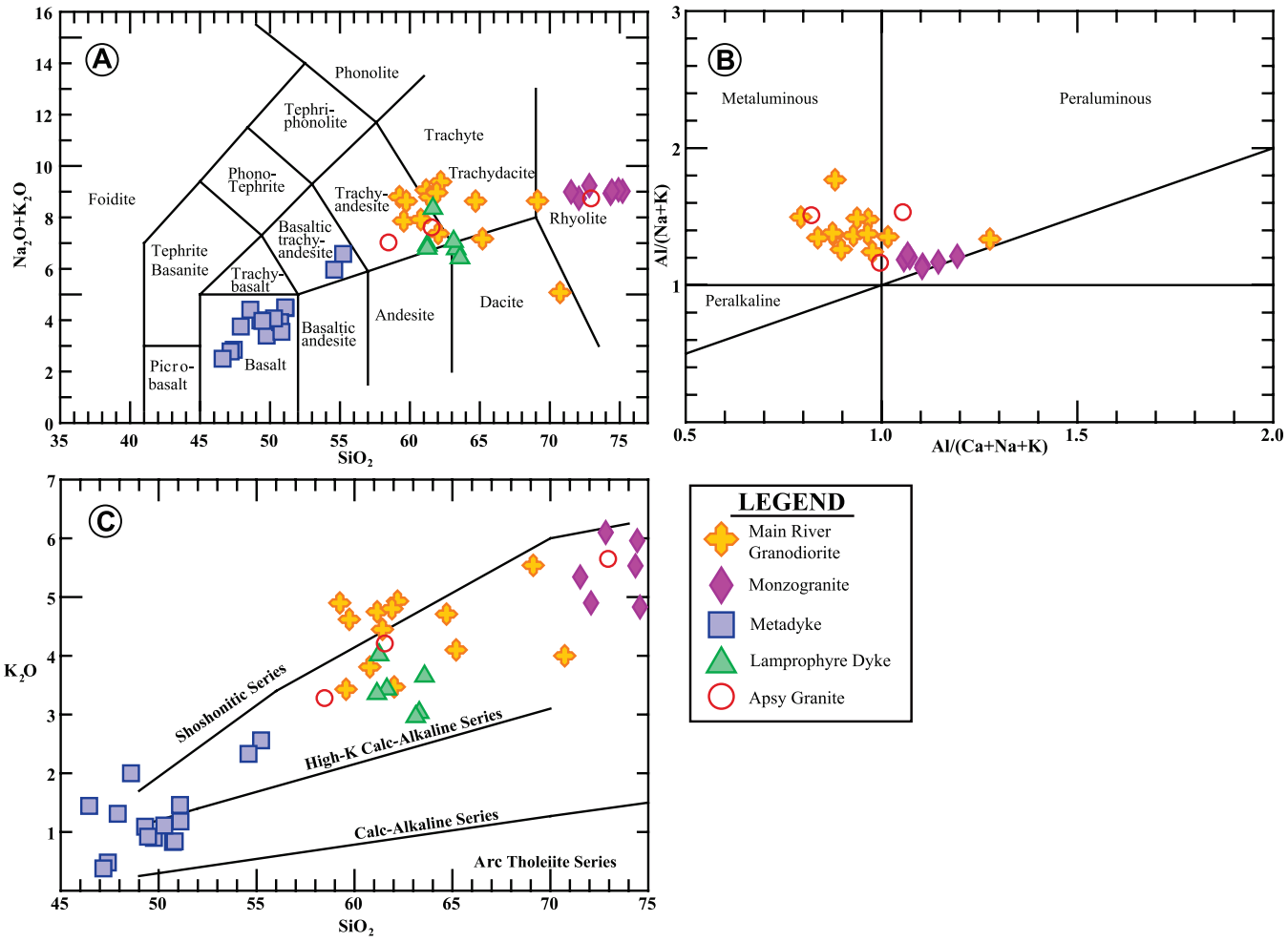

Figure 4. *Major-element classification diagrams. A) Ternary classification diagram after O'Connor (1965) based on CIPW-normative contents of albite, anorthite, and K-feldspar for the granitic rocks at the Viking property. B) Alumina saturation index plot after Shand (1943). The Main River granodiorite and Apsy Granite are metaluminous to weakly peraluminous, whereas the monzogranite sheets are dominantly peraluminous. C) Modified after Peccerillo and Taylor (1976); K_2O versus SiO_2 diagram for the Viking rock types. All but the tholeiitic metadykes plot as High-K calc-alkaline series rocks with the granodiorite containing shoshonitic series-like chemistry.*

^{40}Ar–^{39}Ar THERMOCHRONOLGY

Four samples were collected for ^{40}Ar–^{39}Ar thermochronological analysis; three strongly sericitized granitoids (two monzogranites and one granodiorite) of the Main River Pluton collected within the alteration envelope of the Thor trend, and a strongly foliated phyllite belonging to the Forteau Formation of the Labrador Group. Brief descriptions of the samples and their UTM co-ordinates are presented in Table 3. The two monzogranite samples are heavily fractured and contain 1% disseminated pyrite accompanied by strong pervasive sericite alteration (Plate 3 A, B). Sample 09MM099 is located 10 m north of the Thor vein (Figure 2) and sample 09MM113 is located 200 m south of the Thor vein at the surface. The sericite-altered granodiorite sample is located 15 m northwest of the Thor vein and also contains disseminated pyrite. The phyllite of the Labrador Group is located along the eastern property boundary and was exposed through trenching. It is characterized by a very strong upright dominant foliation defined by aligned, fine-grained sericite, biotite, and quartz (Plate 3C, D). An asymmetric crenulation cleavage and 1- to 2-mm-scale biotite porphyroblasts can be observed on broken foliation surfaces.

In the monzogranite (09MM113 and 09MM099), pervasively sericitized potassium feldspar and plagioclase (Plate 3b) occur intergrown with polycrystalline aggregates of fine-grained quartz. Fine-grained disseminated pyrite is commonly rimmed by magnetite and hematite and associated with the altered feldspars and locally quartz. The granodiorite shows similar alteration mineralogy, however, it

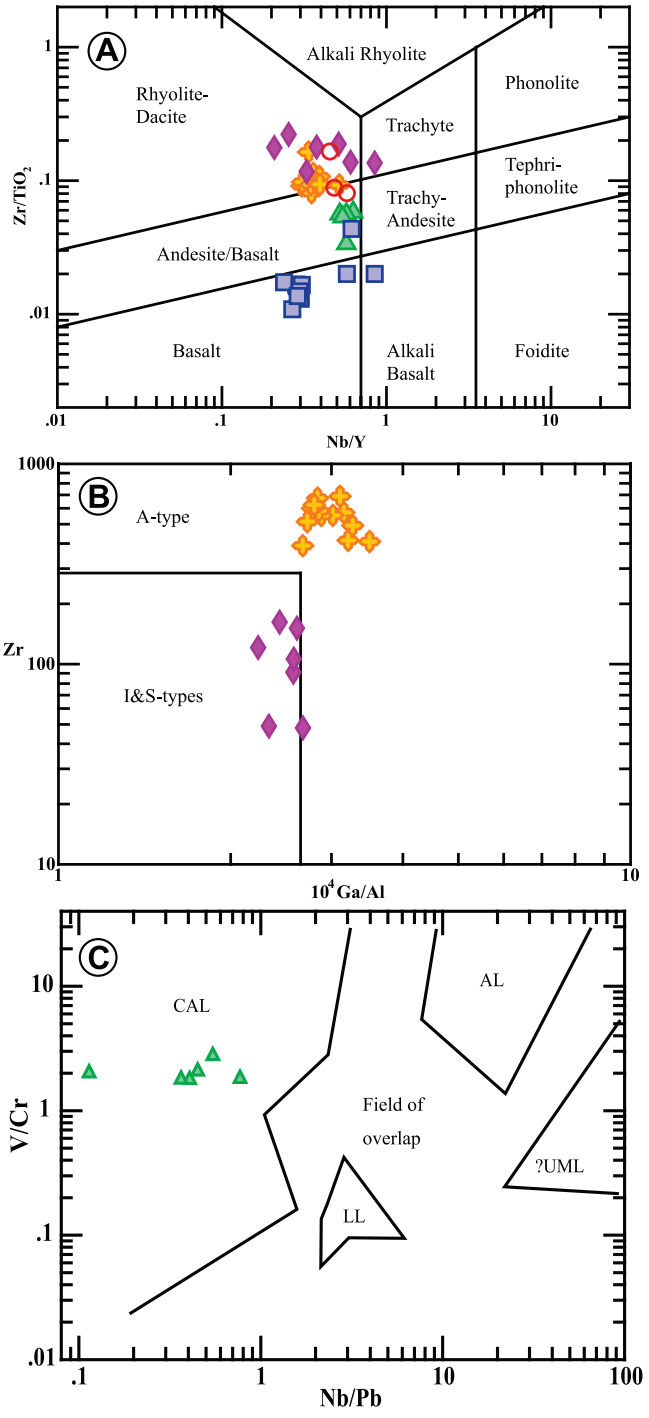

Figure 5. (adjacent) *Trace-element classification diagrams. A) Revised after Winchester and Floyd (1977) after Pearce (1996) plot of the Viking property rock types and granitoid samples from the Apsy Granite. The rocks are generally sub-alkaline (Nb/Y< 0.7) and plot as clusters except for the monzogranite sheets and metadykes. B) Granitoid classification diagram after Whalen* et al. *(1987). The Main River granodiorite contains elevated Zr and Ga/Al; characteristic of A-type granitoid geochemistry. The monzogranites contain lower, but ranging, values of Zr and Ga/Al and plot as I- and S-type granites. C) Discrimination between the 5 lamprophyre branches of Rock (1991) using trace elements. The mesocratic dykes from the Viking property plot as calc-alkaline lamprophyres (CAL). Key: CAL–calc-alkaline lamprophyres, AL–alkaline lamprophyres, LL–lamproites, UML–ultramafic lamprophyres, and KIL–kimberlites. Note logarithmic scales. Fields of overlap represent areas of lower confidence classification. Symbols as Figure 4.*

also locally contains biotite that encloses megacrystic potassium feldspar. The biotite porphyroblasts in the phyllite (09MM024) are typically euhedral, 1 to 2 mm in size, and are set in a strongly foliated matrix of fine- to very fine-grained sericite, recrystallized quartz, and pyrite. A number of the biotite porphyroblasts preserve an internal fabric defined by matrix inclusion trails. Outcrop and petrographic observations indicate that these porphyroblasts record east side down, dextral rotation relative to the surrounding matrix. Locally, however, other biotite porphyroblasts completely overgrow the foliation. The crenulation cleavage observed in outcrop is a smooth, anastamosing, discrete crenulation cleavage composed of sericite and quartz. Pyrite is associated with many mineral phases in the phyllite including the biotite porphyroblasts and sericite alteration.

ANALYTICAL METHODS

The ^{40}Ar–^{39}Ar laser step-heating data were obtained at Queen's University ^{40}Ar–^{39}Ar Thermochronology Laboratory. All weathering surfaces were removed and a fist-sized whole-rock portion of the specimens was carefully milled by mortar and pestle. The crushed material was then sieved to a -40+60 mesh (0.422–0.251 mm) size fraction. The grain separates were ultrasonically agitated in a dilute (2.5 %) solution of reagent grade HNO_3. The samples were frequently cleaned in de-ionized water, dried, and then processed through a Frantz™ isodynamic magnetic separator after a hand magnet was passed over the crushed material. Approximately 500 mg of high-purity biotite and sericite concentrate were packed in aluminium foil and stacked sequentially and interspersed with reference flux monitors of known age (Hb3gr: 1072 Ma; Roddick, 1983). These were evenly spaced with the unknowns, to enable precise determination of the irradiation parameter, "J", throughout the irradiation tube. Unknowns and flux monitors were irradiated with fast neutrons in position 5C for 40 hours (3 MWH) at the McMaster University Reactor, McMaster University, Hamilton, Ontario.

Total-gas, integrated ages (equivalent to a K–Ar age: IA), plateau ages (PA) and inverse isotope-correlation ages

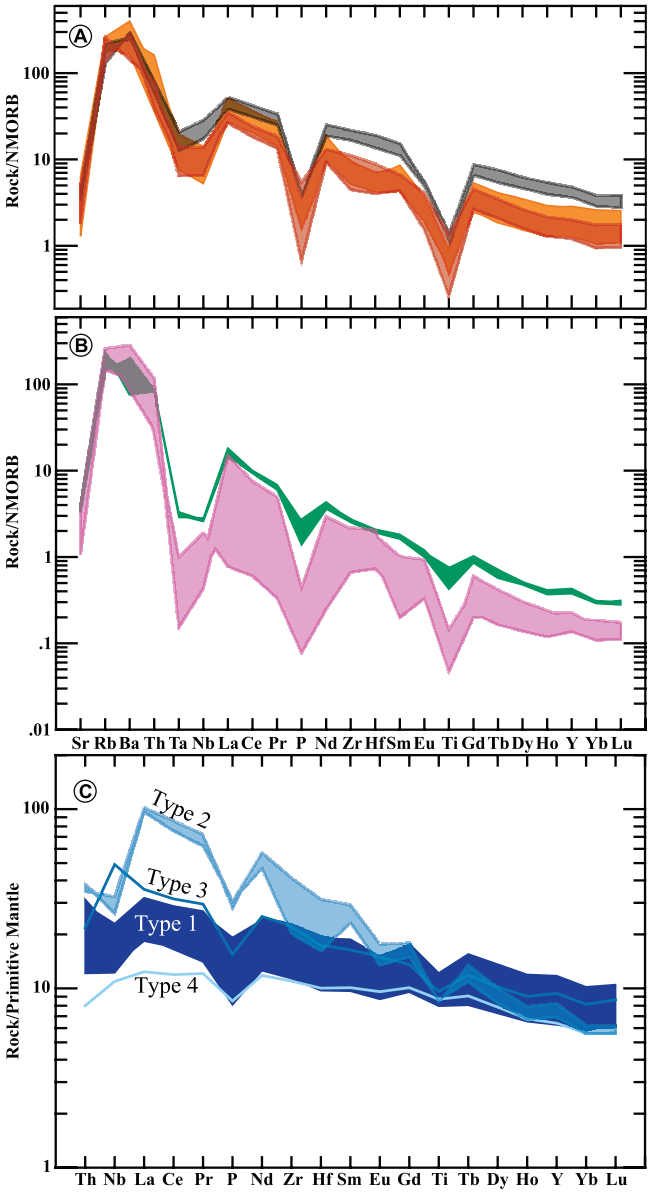

Figure 6. *A) Custom NMORB-normalized multi-element plot for the Main River granodiorite (orange), Apsy Granite (red), and the Potato Hill Pluton (grey;* see *text for discussion). B) Similar plot as (A) but for the monzogranite sheets (pink) and the mesocratic dykes (green). C) Primitive-mantle-normalized multi-element plot for the metadykes. Type 1 is the most dominant with other types exhibiting variations in the LREE and HFSE.*

(CA) are reported. Traditionally, a plateau is defined by three contiguous steps overlapping in error, comprising greater than or equal to 50% of the ^{39}Ar released, and with reasonably low excess scatter (mean square of the weighted deviates (MSWD) <2.2; McDougall and Harrison, 1988; Snee *et al.*, 1988; Singer and Pringle, 1996). These criteria were not satisfied by all of the gas-release spectra for the

Table 3. Rock type, location (UTM, eastings and northings) and brief descriptions of the analyzed samples for ^{40}Ar–^{39}Ar thermochronology. UTM-coordinates are given in NAD27

Sample	UTM co-ordinates[a]			Unit	Mineral	Description[b]	Integrated age (Ma)	Plateau age (Ma)
	Zone	Easting	Northing					
09MM024	21	500998	5504291	Labrador Group	Biotite	Fine-grained biotite porphyroblastic phyllite with strong upright foliation.	418.29 ± 1.45	419.36 ± 1.46
09MM113	21	500598	5504175	Main River Pluton	Muscovite	Strong sericite-pyrite-quartz altered and mineralized monzogranite in Thor Trend.	387.05 ± 1.44	384.26 ± 1.78
09MM099	21	500578	5504453	Main River Pluton	Muscovite	Strong sericite-pyrite-quartz altered and mineralized monzogranite in footwall to Thor Vein.	398.3 ± 1.4	398.9 ± 2.2
09MM098	21	500570	5504457	Main River Pluton	Muscovite	Strong sericite-pyrite-quartz altered and mineralized granodiorite in footwall to Thor Vein.	382.82 ± 1.09	377.10 ± 1.49

[a] - UTM co-ordinates given in NAD27 projection.
[b] - Field description supplemented by petrography.

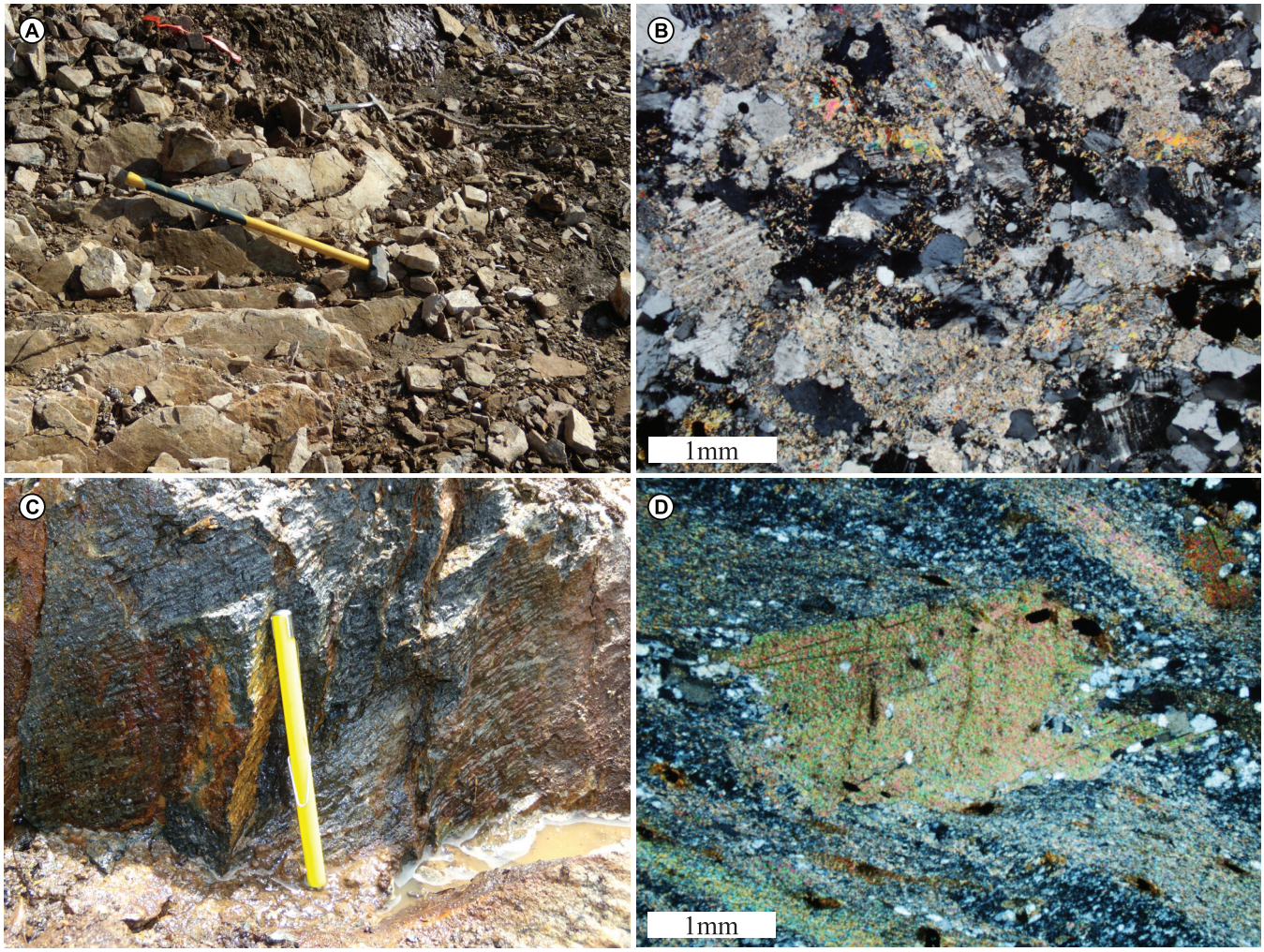

Plate 3. *A) Outcrop photo at the argon sample site (09MM113) of a strongly sericite-altered and folded monzogranite within the Thor trend. Sledge hammer is* ca. *1.2 m in length. B) Photomicrograph of the strongly sericite-altered monzogranite from (A). Feldspars are being replaced by fine-grained sericite (cross-polarized light). C) Outcrop photo of the Forteau Formation phyllite with a shallowly east-dipping fabric and an upright foliation (following pen magnet). (D) Photomicrograph of the same phyllite displaying a rotated biotite porphyroblast with an internal strain fabric (lines running north to south through the biotite) cutting a foliation of quartz, sericite, and pyrite (cross-polarized light).*

samples under investigation. The gas steps used in the calculation of the plateau ages, as well as the inverse isotope-correlation ages, are marked by asterisks in Table 4 and are filled black boxes in Figure 7. The approximate argon closure temperatures for sericite (muscovite: *ca*. 350° C) and biotite (*ca.* 280° C) are applied to these minerals and are used to aid in the interpretation of the cooling history of the host rocks (McDougall and Harrison, 1988; Reynolds, 1992). All age calculations used the ^{40}Ar–^{39}Ar age spectrum module of Ludwig (2003).

STEP-HEATING RESULTS

An aliquot of biotite from the deformed phyllite (09MM024) yielded a very well-defined, consistently flat gas-release spectrum (Figure 7A). The analyses produced a total gas, integrated age of 418 ± 1.5 Ma. Eleven of 14 steps, representing 99.12% of the total ^{39}Ar released, gave a plateau age of 419 ± 1.5 Ma [(MSWD) = 0.84; Probability of Fit (POF) = 0.62] overlapping within error with the integrated age. The corresponding inverse-correlation age (^{36}Ar–^{40}Ar *vs* ^{39}Ar–^{40}Ar) of 418 ± 1.5 Ma (MSWD = 0.84) also overlaps within error with the plateau and integrated ages. These data collectively indicate that an age of 419 ± 1.5 Ma represents a robust cooling age for this biotite and therefore represents the time at which the sample cooled through about 280°C. A simple thermal history is inferred for this sample because of close agreement of integrated, plateau and isotope correlation ages.

Table 4. The ^{40}Ar–^{39}Ar analytical data. Asterisks denote steps excluded from plateau and inverse-correlation age calculations. J-values were determined through interpolation

Power[a]	$^{36}Ar/^{39}Ar$	$^{40}Ar/^{39}Ar$	$\%^{40}Ar$ ATM	$*^{40}Ar/^{39}Ar$	Ca/K	f_{39} [b] (%)	Apparent Age Ma[c]
09MM024 Biotite; J[d] = 0.016889 ± 0.000034							
* 1.8	0.001453 ± 0.001191	0.063083 ± 0.003169	42.83	9.05 ± 5.62	0.000	0.11	256.6 ± 148.6
* 2.0	0.000789 ± 0.000295	0.083174 ± 0.00152	23.24	9.22 ± 1.06	0.012	0.67	261.1 ± 28.1
* 2.2	0.000114 ± 0.000032	0.062978 ± 0.000468	3.37	15.34 ± 0.19	0.007	4.32	415.7 ± 4.5
2.3	0.00004 ± 0.000035	0.063514 ± 0.000583	1.18	15.56 ± 0.22	0.000	4.01	420.9 ± 5.2
2.4	0.000044 ± 0.000024	0.063788 ± 0.000391	1.29	15.47 ± 0.15	0.010	6.37	418.9 ± 3.6
2.5	0.000026 ± 0.000021	0.06425 ± 0.000381	0.76	15.45 ± 0.13	0.015	5.89	418.2 ± 3.2
2.6	0.000011 ± 0.000026	0.064294 ± 0.000433	0.33	15.5 ± 0.16	0.000	5.53	419.5 ± 3.8
2.7	0.000015 ± 0.00004	0.064085 ± 0.000554	0.45	15.53 ± 0.23	0.000	3.55	420.3 ± 5.5
2.9	0.000044 ± 0.000026	0.064051 ± 0.000442	1.31	15.41 ± 0.16	0.015	4.53	417.3 ± 3.9
3.1	0.000015 ± 0.000027	0.063963 ± 0.000555	0.44	15.57 ± 0.18	0.032	6.83	421.1 ± 4.4
3.3	0.000003 ± 0.000022	0.064443 ± 0.000422	0.08	15.51 ± 0.14	0.015	12.44	419.6 ± 3.5
3.5	0.000011 ± 0.000017	0.064554 ± 0.000488	0.34	15.44 ± 0.14	0.016	18.13	418 ± 3.4
3.7	0.00001 ± 0.000018	0.064148 ± 0.000427	0.30	15.54 ± 0.13	0.014	15.96	420.5 ± 3.2
3.9	0.000004 ± 0.000019	0.06445 ± 0.000473	0.13	15.5 ± 0.14	0.017	9.42	419.4 ± 3.5
* 4.2	0.000023 ± 0.000074	0.06282 ± 0.000724	0.68	15.81 ± 0.39	0.091	1.90	427 ± 9.5
* 4.8	0.00005 ± 0.000427	0.058005 ± 0.001718	1.46	16.99 ± 2.25	0.311	0.25	455.1 ± 53.2
* 6.0	0.00051 ± 0.000996	0.049528 ± 0.00214	15.05	17.15 ± 6.02	0.000	0.10	458.8 ± 142.1
09MM113 Sericite; J[d] = 0.016896 ± 0.000034							
* 1.8	0.000324 ± 0.00013	0.025772 ± 0.000707	9.51	35.11 ± 1.79	0.0490	0.64	840.2 ± 34.3
* 2.0	0.000039 ± .000036	0.074391 ± 0.000704	1.15	13.29 ± 0.19	0.0050	5.2	365.4 ± 4.7
* 2.2	0.000011 ± 0.000026	0.074199 ± 0.000549	0.32	13.43 ± 0.14	0.0130	6.9	369 ± 3.6
* 2.3	0.000009 ± 0.000031	0.072614 ± 0.000572	0.27	13.73 ± 0.17	0.0000	5.8	376.5 ± 4.2
2.5	0.000024 ± 0.000029	0.070769 ± 0.000559	0.72	14.03 ± 0.16	0.0250	6.79	383.7 ± 4.1
2.7	0.000036 ± 0.000072	0.071382 ± 0.000647	1.06	13.86 ± 0.33	0.0230	5.57	379.6 ± 8
2.9	0.000026 ± 0.00002	0.070763 ± 0.000413	0.77	14.02 ± 0.12	0.0090	14.37	383.6 ± 2.9
3.0	0.000018 ± 0.000017	0.070702 ± 0.000394	0.54	14.07 ± 0.11	0.0180	25.73	384.7 ± 2.6
3.1	0.000013 ± 0.000022	0.070304 ± 0.000444	0.38	14.17 ± 0.13	0.0170	9.25	387.2 ± 3.2
* 3.2	0.000033 ± 0.000032	0.068929 ± 0.00065	0.97	14.37 ± 0.19	0.0060	5.67	392.1 ± 4.8
* 3.3	0.000037 ± 0.000029	0.068981 ± 0.000595	1.09	14.34 ± 0.18	0.0200	5.52	391.4 ± 4.3
* 3.6	0.000056 ± 0.000068	0.066985 ± 0.000902	1.64	14.68 ± 0.36	0.1140	2.84	399.8 ± 8.8
* 6.0	0.000036 ± 0.000034	0.06811 ± 0.000525	1.06	14.53 ± 0.19	0.0100	5.72	396 ± 4.6
09MM099 Sericite; J[d] = 0.016829 ± 0.000034							
* 1.8	0.000317 ± 0.000092	0.022979 ± 0.000517	9.32	39.46 ± 1.49	0.179	0.84	921.5 ± 27.2
* 2.0	0.000047 ± 0.000042	0.071070 ± 0.000672	1.40	13.87 ± 0.22	0.030	5.28	379.8 ± 5.4
* 2.2	0.000022 ± 0.000026	0.073014 ± 0.000590	0.65	13.61 ± 0.15	0.020	8.11	373.2 ± 3.8
* 2.3	0.000022 ± 0.000039	0.072458 ± 0.000597	0.65	13.71 ± 0.20	0.037	5.32	375.8 ± 4.9
* 2.5	0.000039 ± 0.000031	0.071194 ± 0.000614	1.16	13.88 ± 0.18	0.050	6.82	380.1 ± 4.4
* 2.7	0.000038 ± 0.000025	0.070340 ± 0.000411	1.13	14.06 ± 0.13	0.044	7.57	384.3 ± 3.3
* 2.8	0.000027 ± 0.000020	0.068624 ± 0.000460	0.79	14.46 ± 0.13	0.039	16.19	394.2 ± 3.2
* 2.9	0.000035 ± 0.000021	0.067323 ± 0.000490	1.04	14.70 ± 0.14	0.039	13.45	400.1 ± 3.5
* 3.0	0.000025 ± 0.000020	0.068043 ± 0.000482	0.75	14.59 ± 0.14	0.032	11.83	397.4 ± 3.3
* 3.1	0.000034 ± 0.000029	0.067488 ± 0.000535	1.00	14.67 ± 0.17	0.041	7.34	399.4 ± 4.2
3.2	0.000054 ± 0.000024	0.065466 ± 0.000465	1.57	15.03 ± 0.15	0.067	7.95	408.3 ± 3.7
3.3	0.000104 ± 0.000080	0.064199 ± 0.000762	3.05	15.10 ± 0.41	0.102	2.30	409.9 ± 10.0
3.6	0.000078 ± 0.000082	0.065899 ± 0.000832	2.29	14.83 ± 0.41	0.096	2.22	403.2 ± 10.1
6.0	0.000058 ± 0.000044	0.064951 ± 0.000627	1.72	15.13 ± 0.25	0.060	4.78	410.6 ± 6.0
09MM098 Sericite; J[d] = 0.016894 ± 0.000034							
* 1.6	0.000798 ± 0.000509	0.015801 ± 0.000966	23.48	48.42 ± 10.11	0.118	0.04	1078.3 ± 169.6
* 1.9	0.000244 ± 0.000114	0.021300 ± 0.000582	7.11	43.61 ± 2.00	0.169	0.18	995.8 ± 35.1
* 2.1	0.000052 ± 0.000020	0.067359 ± 0.000489	1.52	14.62 ± 0.14	0.503	4.56	398.2 ± 3.4
* 2.3	0.000026 ± 0.000017	0.073414 ± 0.000424	0.76	13.52 ± 0.11	0.641	7.14	371.1 ± 2.6
2.5	0.000015 ± 0.000020	0.072440 ± 0.000624	0.44	13.74 ± 0.15	0.162	7.50	376.7 ± 3.6
2.7	0.000015 ± 0.000020	0.072317 ± 0.000502	0.44	13.77 ± 0.13	0.063	7.07	377.3 ± 3.1
2.8	0.000011 ± 0.000024	0.072598 ± 0.000497	0.34	13.73 ± 0.14	0.042	4.99	376.3 ± 3.4
2.9	0.000018 ± 0.000020	0.072562 ± 0.000464	0.54	13.71 ± 0.12	0.056	4.58	375.8 ± 3.0
3.0	0.000010 ± 0.000016	0.072288 ± 0.000478	0.30	13.79 ± 0.11	0.040	6.66	377.9 ± 2.8
3.1	0.000016 ± 0.000015	0.072103 ± 0.000481	0.48	13.80 ± 0.11	0.046	6.76	378.1 ± 2.7
* 3.2	0.000014 ± 0.000017	0.071447 ± 0.000503	0.40	13.94 ± 0.12	0.026	9.37	381.5 ± 3.0
* 3.3	0.000009 ± 0.000014	0.071406 ± 0.000454	0.26	13.97 ± 0.11	0.033	8.48	382.2 ± 2.6
* 3.4	0.000020 ± 0.000018	0.071183 ± 0.000425	0.57	13.97 ± 0.11	0.027	7.03	382.2 ± 2.8
* 3.5	0.000008 ± 0.000017	0.070833 ± 0.000512	0.24	14.08 ± 0.13	0.060	7.45	385.1 ± 3.1
* 3.7	0.000013 ± 0.000019	0.070691 ± 0.000485	0.37	14.09 ± 0.13	0.099	6.64	385.3 ± 3.1
* 3.9	0.000016 ± 0.000019	0.070413 ± 0.000485	0.47	14.14 ± 0.13	0.103	3.81	386.3 ± 3.1
* 4.2	0.000011 ± 0.000034	0.070265 ± 0.000529	0.31	14.19 ± 0.18	0.086	2.45	387.6 ± 4.4
* 6.0	0.000017 ± 0.000018	0.070057 ± 0.000434	0.50	14.20 ± 0.12	0.065	5.30	388.0 ± 2.9

a - As measured by laser in % of full nominal power (10W)
b - Fraction ^{39}Ar as percent of total run
c - Errors are analytical only and do not reflect error in irradiation parameter J
d - Nominal J-value, referenced to PP-20 (Hb3gr) = 1072 Ma (Roddick, 1983)
* - Step not inculded in plateu or inverse isotope correlation age determination
All uncertainties quoted at 2σ level

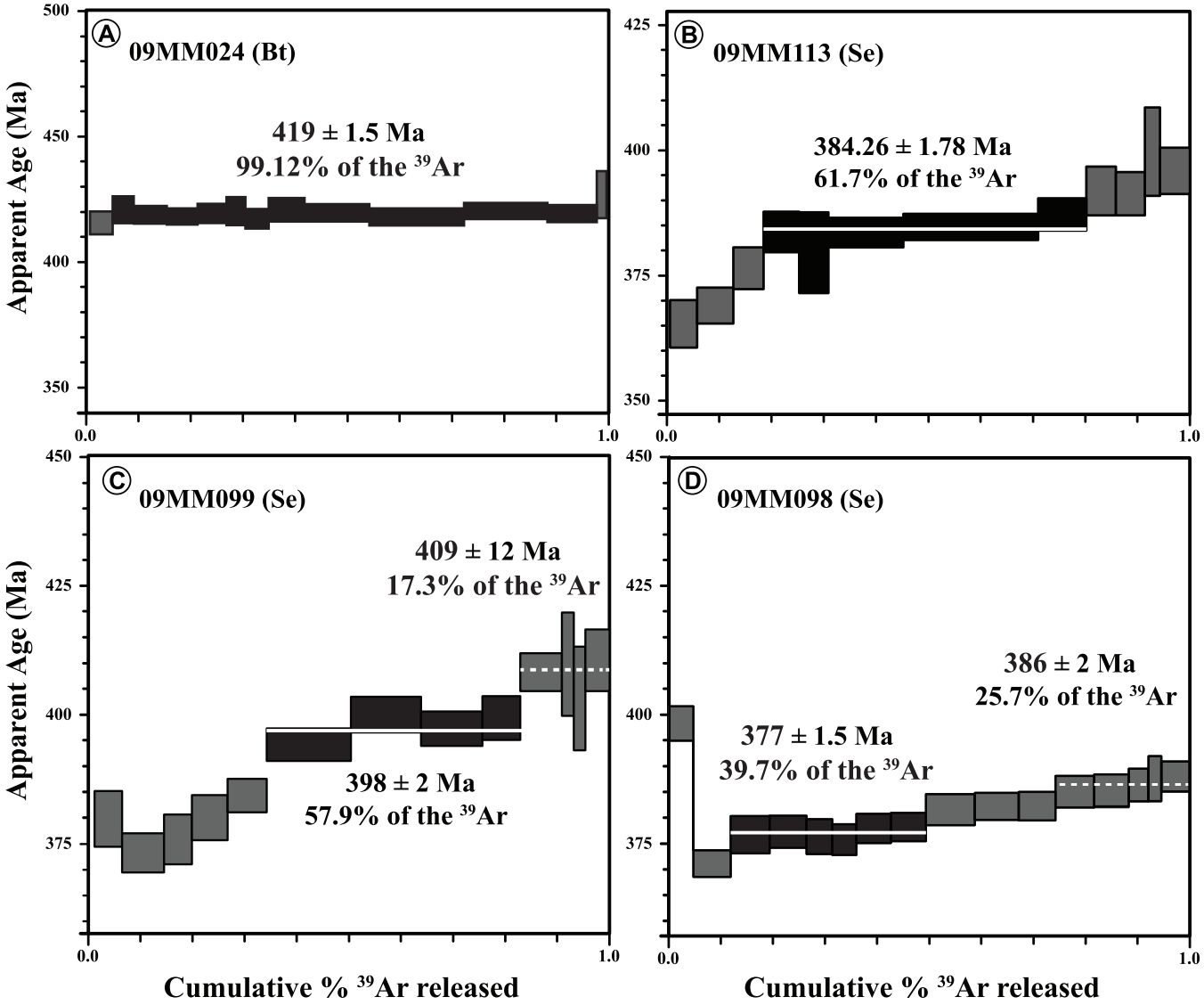

Figure 7. *The ^{40}Ar–^{39}Ar release spectra for biotite (A) and sericite (B-D) plotted as apparent age (Ma)* vs *cumulative percent ^{39}Ar released. Dashed white lines represent higher power pseudo-plateaus that may better approximate the primary argon cooling age of the sample. Solid white lines represent pseudo-plateaus that may suggest partial resetting of the ^{40}A–^{39}Ar systematics during later hydrothermal events. Gas steps used in the calculation of plateaus and inverse isotope correlation ages are black, those not used in calculations are grey.*

A single aliquot of fine-grained sericite concentrate from sample 09MM113 produced a well-defined argon release spectrum with young ages recorded in the low-power gas steps, a series of mutually consistent steps in the middle and significantly older ages produced at higher power (Figure 7B). Five of thirteen gas steps, representing 61.7% of the ^{39}Ar released yielded a plateau age of 384 ± 1.8 Ma (MSWD = 1.2; POF = 0.30). An inverse isotope correlation age for the same 5 steps of 364 ± 21 Ma is significantly younger than, but overlaps within error, the plateau age. The plateau age is therefore interpreted as a reasonable estimate of the cooling age when the sericite passed through about 350° C (McDougall and Harrison, 1988 and references therein; Snee *et al.*, 1988; Singer and Pringle, 1996).

Sericite from another monzogranite sample (09MM099) yielded a poorly defined argon release spectra (Figure 7C). The pattern for this sample is comparable to that of sample 09MM113 with young ages at low power, a pseudo-plateau through the middle and an older pseudo-plateau segment at higher power. The pseudo-plateau age of 398.9 ± 2.2 Ma for the central segment represents 57.9% of the ^{39}Ar released during four steps (MSWD = 0. 68, POF = 0.51). The higher power pseudo-plateau segment represent-

ing only 17.3% of the ^{39}Ar released (MSWD= 0.034: POF= 0.992), yielded an age of 409 ± 12 Ma. The incrementally ascending spectrum for this specimen suggests that the higher power gas steps may represent a maximum age of gold deposition. This age overlaps within error the age constraints on the mineralization at the Rattling Brook deposit (Kerr and van Breemen, 2007). The younger, lower power, gas-release steps suggest partial resetting of the ^{40}Ar–^{39}Ar systematics during a younger hydrothermal event at *ca.* 380 Ma.

A sample of a sericite-altered granodiorite (09MM098) produced a gas release spectrum very similar to that of 09MM099 in having incrementally increasing ages for higher power gas-release steps. The high power pseudo-plateau consisting of five of eighteen steps and representing 25.7% of the ^{39}Ar released gave an age of 386 ± 2 Ma (MSWD = 0.68, POF = 0.60). The lower power pseudo-plateau, comprising six of eighteen steps and representing only 37.9% of the total ^{39}Ar released (MSWD = 0.38; POF = 0.86: Figure 7D) yielded an age of 377 ± 2 Ma. This spectrum suggests a *ca.* 388 Ma primary cooling age for the sericite, but that this has been partially reset during later, *ca.* 377 Ma hydrothermal activity.

DISCUSSION

Orogenic gold deposits are characterized by quartz-dominant vein systems with ≤3–5% sulphide minerals (typically Fe-sulphides) and ≤5–15% carbonate minerals (Groves *et al.*, 1998). Pyrite (and/or pyrrhotite) is the most common sulphide in deposits hosted in metamorphosed igneous rocks and gold-bearing veins exhibit variable enrichments in As, B, Bi, Hg, Sb, Te, and W; Cu, Pb, and Zn concentrations are generally only slightly elevated above regional backgrounds (Groves *et al.*, 1998). The veins within the Thor trend contain Cu, Pb, Zn, Ag, and Cr concentrations above regional background with Au/Ag overlapping the typical range for these deposit types. Silver-rich gold grains are present throughout the mineralized veins, but the absence of arsenopyrite is striking considering its correlation with gold and its abundance in the Rattling Brook deposit (Saunders and Tuach, 1988, 1991; Kerr, 2005). The presence of base metals within the high-grade veins at the Viking property is a noted difference from what is observed at Rattling Brook. This sulphide assemblage may indicate a possible affinity with mineralization observed in the Browning Mine and Unknown Brook deposits (Figure 1B). The absence of arsenopyrite, the 'free' and non-refractory nature of the gold, and a gold recovery of 97% *via* cyanide leaching at a 59 micron grind size (Ebert, 2010), are favourable features amenable to standard ore-processing techniques.

The Main River granodiorite has a calc-alkaline, arc-like, A-type geochemical signature. Halogen enrichments (*e.g.,* F >1000 ppm), a ferroan composition along with high Ga/Al, and Zr, are typical of relatively anhydrous, lower crustal, within plate, A-type granitic magmas typical of deep-crustal anorogenic extensional environments (Pearce *et al.*, 1984; Frost *et al.*, 2001). Other Grenvillian granitoid plutons of the LRI, such as the Apsy Granite and the Lake Michael Intrusive Suite (Owen, 1991), were emplaced contemporaneously with and have geochemical features similar to the Main River Pluton. These plutons were emplaced over a period of *ca.* 50 my, between 1032 and 985 Ma, and are termed Group 1 and Group 2 granitoids, respectively, (Heaman *et al.*, 2002). The A-type nature of all of these roughly synchronous granite suites suggests an interval of deep-crustal anatectic granitoid plutonism during the emplacement of Group 1 granitoids into the LRI.

The monzogranite sheets are slightly peraluminous and have calc-alkaline affinities with LIL element enrichment. They are volcanic-arc granitoids and straddle the divide with syn-collisional granites (Figure 8). These granites are very different from those of the A-type Main River granodiorite and appear to be residual granitic liquids that have fractionated REE-bearing accessory phases. As the monzogranite sheets locally crosscut fabrics observed in the granodiorite, they may be contemporaneous with the younger, *ca*. 1000 Ma, Group 2 granitic rocks of the LRI (Heaman *et al.*, 2002).

The metadykes exposed on the Viking property are within-plate, continental tholeiitic basalts exhibiting variably developed negative HFS element anomalies (Figure 6C). Variable LREE, Nb, and HFSE abundances suggest that several different magma types are represented among these metadykes. Their general northeast-trending orientation and geochemical signature correlates them with the *ca*. 615 Ma Long Range Dykes (Kamo *et al.*, 1989). The Long Range Dykes are interpreted to represent a period of rifting of the Grenvillian continental crust during the opening of the proto-Atlantic ocean.

Globally, calc-alkaline lamprophyres are thought to overlap gold mineralization in both space and time (Rock, 1991). Rock (1991) suggested that because of their unusual mineralogy and bulk chemistry (*e.g*., high LIL elements, CO_2, Ba, and moderate S), lamprophyric melts are similar to mineralizing fluids and they may easily transport gold. Although the absolute timing of the crystallization of the calc-alkaline mesocratic lamprophyres associated with the mineralized Thor vein array is not constrained, field and textural evidence suggest they were rapidly emplaced, either pre- or syn-vein formation and gold deposition.

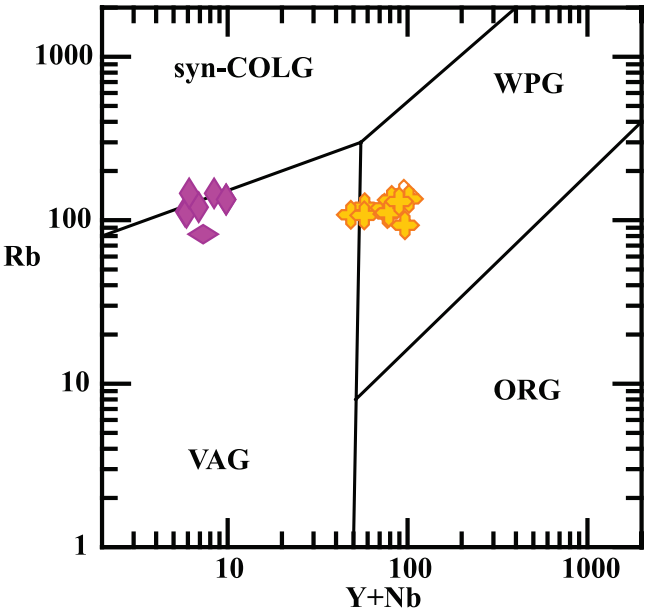

Figure 8. *Tectonomagmatic discrimination diagram after Pearce* et al. *(1984) for the granites of the Viking property. The Main River granodiorite exhibits within-plate trace-element geochemistry, whereas the monzogranite displays a volcanic-arc signature. Symbols as in Figure 4.*

TIMING OF GOLD DEPOSITION AT VIKING

The minimum age of last, peak metamorphism has been constrained through analysis of syn- to late-kinematic biotite porphyroblasts in a phyllitic schist located to the east of the property. The biotite cooled through about 280°C in the Upper Silurian at 419 ± 1.5 Ma. This determination overlaps, within error, the *ca.* 425 ± 10 Ma age of emplacement of the Devil's Room Granite to the north. The syn- to post-kinematic nature of the biotite porphyroblasts suggests that peak metamorphism likely occurred during emplacement of the Devil's Room Granite and the region then rapidly cooled through about 280°C. Latest high-T deformation along this segment of the DVFS therefore occurred during the Late Silurian, corresponding to the Salinic orogeny.

Textural evidence indicates that gold-electrum mineralization is intergrown with hydrothermal sericite. The ^{40}Ar–^{39}Ar thermochronological analysis of sericite from altered rocks in the Thor trend produced a range of cooling ages (Plate 3). The Late Silurian to Early Devonian pseudo-plateau age of 409 ± 12 Ma overlaps within error with the minimum age of peak metamorphism (*ca.* 419 Ma), the emplacement age for the Devil's Room Granite, and correlates with the timing of gold mineralization at the Rattling Brook deposit. This *ca.* 409 Ma age may best approximate the age of gold deposition at the Viking property; however, it may suggest that the mineralization may, in fact be older than 409 Ma. The Early to Middle Devonian incrementally step-wise increasing gas release spectra and their contained pseudo-plateaus (Figure 7 B–D) are inferred to represent the products of partial resetting of hydrothermal sericite (~350° closure temperature) during later fluid flow, alteration and possible gold deposition events. Unpublished fluid-inclusion analysis for the Thor vein suggests that the fluids responsible for deposition of the vein array formed at about 260–320°C at depths of 5–10 km. This temperature range and the uncertainties in the results (± 50˚) overlap with the closure temperature for sericite–muscovite. These data are therefore permissible with the proposal that the sericite and gold were initially deposited at *ca.* 409 Ma (oldest high power steps in the three spectra) and that the sericite has been partially reset during later hydrothermal events (lower power steps).

On a regional scale throughout the northern Appalachian Orogen, the age of gold mineralization at the Viking property correlates with those acquired from the Nugget Pond deposit (Sangster and Pollard, 2001; Sangster *et al.*, 2007) and are within error of the Dufferin deposit in Nova Scotia (Morelli *et al.*, 2005). These deposits have been constrained to the Upper Devonian, broadly corresponding to the waning stages of the Acadian orogeny and onset of the Neoacadian orogeny (van Staal, 2007).

CONCLUSIONS

Gold-electrum mineralization at the Viking property is hosted by quartz ± calcite + sulphide veins and disseminated within the surrounding sericite-altered host rocks. This mineralization corresponds to Type 1 mineralization of Saunders (1991). The veins exhibit a simple sulphide assemblage of pyrite, galena, sphalerite, and chalcopyrite, locally with native silver. Arsenopyrite does not occur at the Viking property. Gold-electrum mineralization in the veins occurs as both 'free' blebs and as inclusions within sulphides; it is not refractory, and has favourable recovery characteristics.

The Main River granodiorite exhibits calc-alkaline within-plate chemistry similar to other Grenvillian granitic plutons that have intruded the external LRI, and has been crosscut by peraluminous I-type monzogranites similar to the equigranular granites within the Potato Hill Pluton (Owen *et al.*, 1992). Calc-alkaline, strongly altered and mineralized, lamprophyre dykes are associated with the mineralized veins and are comparable in composition to the spessartite Weekend Dykes of the Meguma Zone (Tate and Clarke, 1993).

The ^{40}Ar–^{39}Ar cooling ages from biotite and sericite provide constraints on the age of peak metamorphism and gold mineralization at the Viking property. Peak metamorphism

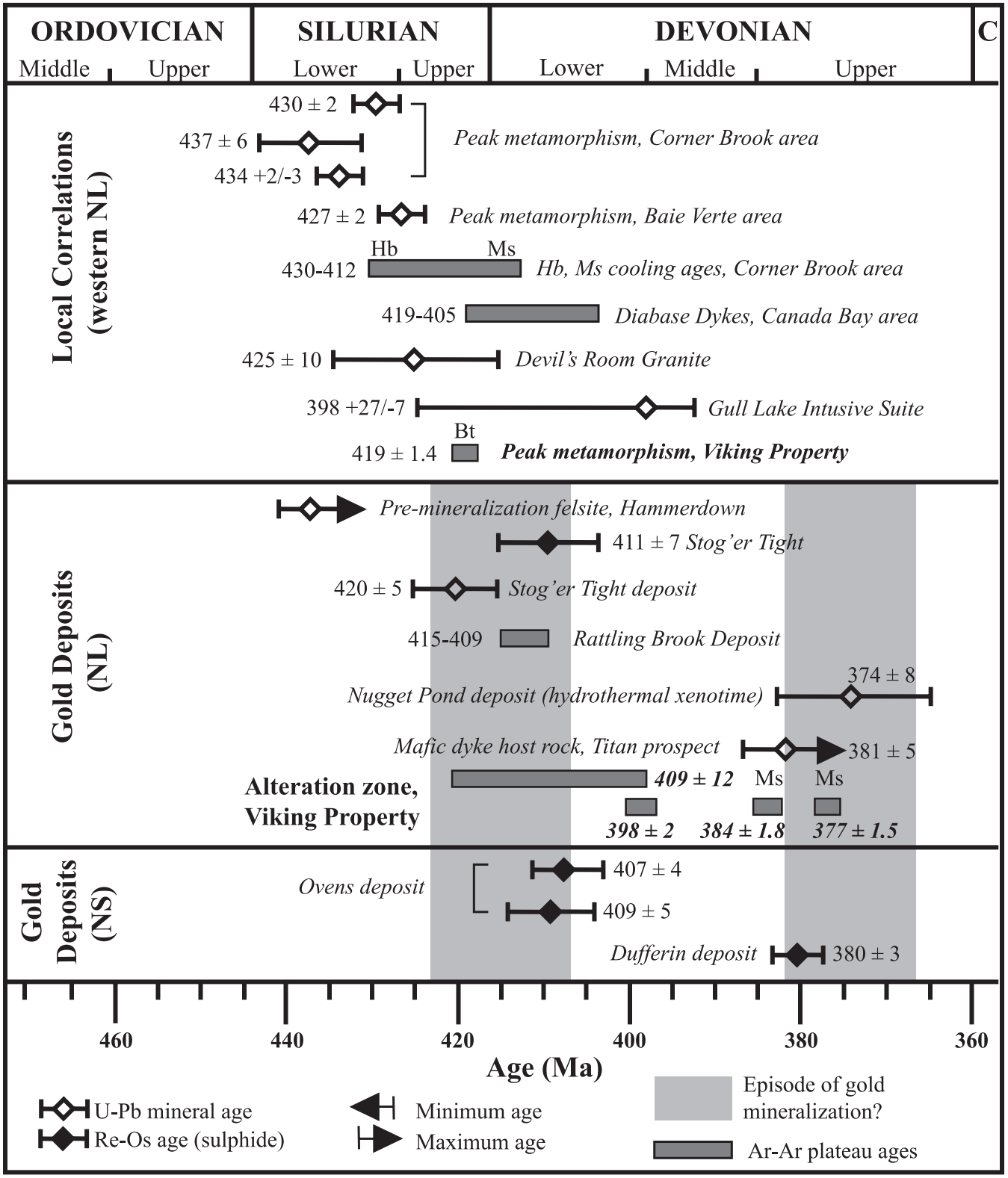

Figure 9. *Summary chart modified after Kerr and van Breeman (2007) displaying the results of ^{40}Ar–^{39}Ar dating at the Viking property and its correlations with other geochronological constraints on the timing of gold deposition, metamorphism, and plutonism in the White Bay area of western Newfoundland, as well as ages for other deposits throughout Newfoundland and Nova Scotia.*

recorded in syn-late kinematic biotite porphyroblasts in the adjacent Labrador Group (*ca.* 419 Ma) corresponds to the waning stages of the Silurian Salinic orogeny and gold-electrum mineralization is best constrained to the Middle to Late Devonian correlating with the onset of Acadian deformation. Less well-defined cooling ages suggest the possibility of a continuum across the two broadly defined periods of gold deposition, at least for the White Bay area, resulting from long-lived displacement and fluid flow along the DVFS, which may reset the Ar systematics for sericite.

ACKNOWLEDGMENTS

Dr. Shane Ebert of Northern Abitibi Mining Corporation is thanked for access to company data. This study would not have been possible without financial and technical support from the Geological Survey Branch of the Department of Natural Resources, Government of Newfoundland and Labrador. Funding for M. Minnett is also provided through an NSERC grant to D. Wilton and the School of Graduate Studies Fellowship, MUN. D. Archibald at Queen's University is thanked for acquisition of the ^{40}Ar–^{39}Ar thermochronological data used in this study. John Hinchey and Andy Kerr are kindly thanked for reviewing the manuscript.

REFERENCES

Cassidy, K.F., Groves, D.I. and McNaughton, N.J.
1998: Late-Archean granitoid-hosted lode-gold deposits, Yilgarn Craton, Western Australia: Deposit characteristics, crustal architecture and implications for ore genesis. Ore Geology Reviews, Volume 13, pages 65-102.

Churchill, R. and Voordouw, R.
2006: First, second, third, and fourth year assessment report documenting reconnaissance prospecting and compilation for map staked licenses 09287M (Wizard Property) and 08878M, 10935M, and 12734M (Viking Property), White Bay area, Newfoundland, NTS Sheets 12H/10 and 12H/11. Assessment Report for Altius Resources Inc, pages 1-137.

Ebert, S.
2008-2011: News releases. Accessed in 2011, from http://www.naminco.ca/news.php

2010: Northern Abitibi announces 97% gold recovery from preliminary metallurgical test work at Viking. Accessed in 2011, from http://www.naminco.ca/docs/NR10-10%20NAI%20Metallurgy%20Release.pdf

2011: Northern Abitibi announces new resource estimate for Viking with 55% increase in gold grade and 80% of original ounces upgraded from inferred to indicated category, News Release, pages 1-3.

Finch, C.J.
1998: Inductively coupled plasma-emission spectrometry (ICP-ES) at the geochemical laboratory. *In* Current Research. Newfoundland Department of Mines and Energy, Report 98-1, pages 179-193.

French, V.A.
1987: Assessment report on 1987 exploration program licences 2831 and 2836, NTS 12H/10 and 12H/11, Silver Mountain for Noranda Exploration Company Limited. [012H-0995], 77 pages.

Frost, B.R., Barnes, C.G., Collins, W.J., Arculus, R.J., Ellis, D.J. and Frost, C.D.
2001: A geochemical classification for granitic rocks. Journal of Petrology, Volume 42, pages 2033-2048.

Grant, J.A.
1986: The isocon diagram - a simple solution to Gresens' equation for metasomatic alteration. Economic Geology, Volume 81, pages 1976-1982.

Groves, D.I., Goldfarb, R.J., Gebre-Mariam, M., Hagemann, S.G. and Robert, F.
1998: Orogenic gold deposits: A proposed classification in the context of their crustal distribution and relationship to other gold deposit types. Ore Geology Reviews, Volume 13, pages 7-27.

Groves, D.I., Goldfarb, R.J., Robert, F. and Hart, C.J.R.
2003: Gold deposits in metamorphic belts: overview of current understanding, outstanding problems, future research, and exploration significance. Economic Geology, Volume 98, pages 1-29.

Heaman, L.M., Erdmer, P. and Owen, J.V.
2002: U–Pb geochronologic constraints on the crustal evolution of the Long Range Inlier, Newfoundland. Canadian Journal of Earth Sciences, Volume 39, pages 845-865.

Hinchey, A.M. and Knight, I.
2011: Early Appalachian thrusting of paleozoic metasediments within a proterozoic basement massif of the southern Long Range Inlier of Newfoundland. Geological Association of Canada Abstracts, Ottawa.

Irvine, T.N. and Baragar, W.R.A.
1971: A guide to the chemical classification of the common volcanic rocks. Canadian Journal of Earth Sciences, Volume 8, pages 523-548.

Kamo, S., Gower, C.F. and Krogh, T.E.
1989: A birthdate for the Iapetus ocean? A precise U-Pb zircon and baddeleyite age for the Long Range Dykes, S.E. Labrador. Geology, Volume 17, pages 602-605.

Kerr, A.
2005: Geology and geochemistry of unusual gold mineralization in the Cat Arm Road area, western White Bay: Preliminary assessment in the context of new exploration models. *In* Current Research. Newfoundland and Labrador Department of Natural Resources, Geological Survey, Report 05-1, pages 173-206.

2006a: Mesothermal gold mineralization in the Silurian Sops Arm group, western Newfoundland: A descriptive and historical overview. *In* Current Research. Newfoundland and Labrador Department of Natural Resources, Geological Survey, Report 06-1, pages 61-90.

2006b: Silurian Rocks of the Sops Arm group, western Newfoundland: Some new food for future digestion. *In* Current Research. Newfoundland and Labrador Department of Natural Resources, Geological Survey, Report 06-1, pages 91-117.

Kerr, A. and van Breemen, O.
2007: The timing of gold mineralization in White Bay, western Newfoundland: Evidence from ^{40}Ar-^{39}Ar studies of mafic dykes that predate and postdate mineralization. Atlantic Geology, Volume 43, pages 148-162.

Kerrich, R.
1993: Perspectives on genetic models for lode gold deposits. Mineralium Deposita, Volume 28, pages 362-365.

Ludwig, K.R.
2003: ISOPLOT 3.0: A geochronological toolkit for Microsoft Excel. Geochronology Center Special Publication, Volume 4, page 71.

Macdonald, R., Thorpe, R.S., Gaskarth, J.W. and Grindrod, A.R.
1985: Multi-component origin of Caledonian lamprophyres of northern England. Mineralogical Magazine, Volume 49, pages 485-494.

Mauger, R.L.
1988: Geochemical evidence for sediment recycling from North Carolina (U.S.A.) minettes. Canadian Mineralogist, Volume 26, pages 133-141.

McCuaig, C.T. and Kerrich, R.
1998: P-T-t-deformation-fluid characteristics of lode gold deposits: evidence from alteration systematics. Ore Geology Reviews, Volume 12, pages 381-453.

McDougall, I. and Harrison, T.M.
1988: Geochronology and thermochronology by the ^{40}Ar-^{39}Ar method. Oxford Monographs on Geology and Geophysics #9, Oxford, United Kingdom, Oxford University Press, 212 pages.

Minnett, M., Sandeman, H.A. and Wilton, D.
2010: Regional setting of gold mineralization at the Viking property, southern White Bay, Newfoundland. *In* Current Research. Newfoundland and Labrador Department of Natural Resources, Report 10-1, pages 51-64.

Morelli, R.M., Creaser, R.A., Selby, D., Kontak, D.J. and Horne, R.J.
2005: Rhenium-osmium geochronology of arsenopyrite in Meguma Group gold deposits, Meguma Terrane, Nova Scotia, Canada: Evidence for multiple gold-mineralizing events. Economic Geology, Volume 100, pages 1229-1242.

O'Connor, J.T.
1965: A classification for quartz-rich igneous rocks based on feldspar ratios. *In* US Geological Survey Professional Paper B525. USGS, pages 79-84.

Owen, J.V.
1991: Geology of the Long Range Inlier, Newfoundland. Geological Survey of Canada, Bulletin 395, pages 1-97.

Owen, J.V., Greenough, J.D., Fryer, B.J. and Longstaffe, F.J.
1992: Petrogenesis of the Potato Hill pluton, Newfoundland: transpression during the Grenvillian orogenic cycle? Journal of the Geological Society, London, Volume 149, pages 923-935.

Pearce, J.A.
1996: A user's guide to basalt discrimination diagrams. Geological Association of Canada Short Course Notes, Volume 12, pages 79-113.

Pearce, J.A., Harris, N.B.W. and Tindle, A.G.
1984: Trace element discrimination diagrams for the tectonic interpretation of granitic rocks. Journal of Petrology, Volume 25, pages 956-983.

Peccerillo, A. and Taylor, S.R.
1976: Geochemistry of Eocene calc-alkaline volcanic rocks from the Kastamonu area, northern Turkey. Contributions to Mineralogy and Petrology, Volume 58, pages 53-61.

Reynolds, P.H.
1992: Low temperature thermochronology by the ^{40}Ar-^{39}Ar method. *In* Low Temperature Thermochronology. *Edited by* M. Zentilli and P.H. Reynolds. Mineralogical Association of Canada, pages 3-19.

Rock, N.M.S.
1991: Lamprophyres. Glasgow, UK, Blackie.

Roddick, J.C.
1983: High precision intercalibration of ^{40}Ar-^{39}Ar standards. Geochimica et Cosmochimica Acta, Volume 47, pages 887-898.

Sangster, A.L., Douma, S.L. and Lavigne, L.
2007: Base metal and gold deposits of the Betts Cove Complex, Baie Verte Peninsula, Newfoundland. *In* Mineral Deposits of Canada: A Synthesis of Major Deposit Types, District Metallogeny, The Evolution of Geological Provinces and Exploration Methods. *Edited by* W.D. Goodfellow. Geological Survey of Canada, Mineral Deposits Division, Special Volume 5, pages 703-721.

Sangster, A.L. and Pollard, D.
2001: Field guide to mineral occurrences in the Betts Cove and Tilt Cove areas, Newfoundland. *In* Geology and Mineral Deposits of the Northern Dunnage Zone, Newfoundland Appalachians. *Edited by* D.T.W. Evans and A. Kerr. GAC-MAC-CSPG Annual Meeting, St. John's, Newfoundland, 2001, Field Trip Guide A2, pages 37-51.

Saunders, C.M.
1991: Mineralization in western White Bay. *In* Current Research. Newfoundland Department of Mines and Energy, Report 91-1, pages 335-347.

Saunders, C.M. and Tuach, J.
1988: K-Feldspathization, albitization and gold mineralization in granitoid rocks: The Rattling Brook alteration system, western White Bay, Newfoundland. *In* Current Research. Newfoundland Department of Mines and Energy, Mineral Development Division, Report 88-1, pages 307-317.

1991: Potassic and sodic alteration accompanying gold mineralization in the Rattling Brook deposit, western White Bay, Newfoundland Appalachians. Economic Geology, Volume 86, pages 555-569.

Shand, S.J.
1943: Eruptive Rocks. Their Genesis, Composition, Classification, and their Relation to Ore-Deposits with a Chapter on Meteorite. New York, Wiley & Sons.

Singer, B.S. and Pringle, M.S.
1996: Age and duration of the Matuyama-Brunhes geomagnetic polarity reversal from 40Ar-39Ar incremental heating analyses of lavas. Earth and Planetary Science Letters, Volume 139, pages 47-61.

Smyth, W.R. and Schillereff, H.S.
1982: The Pre-Carboniferous geology of southwest White Bay. *In* Current Research. Newfoundland Department of Mines and Energy, Report 82-1, pages 78-98.

Snee, L.W., Sutter, J.F. and Kelly, W.C.
1988: Thermochronology of economic mineral deposits; dating the stages of mineralization at Panasqueira, Portugal, by high-precision 40 / 39 Ar age spectrum techniques on muscovite. Economic Geology, Volume 83, pages 335-354.

Strong, D.F.
1974: Plateau lavas and diabase dykes of northwestern Newfoundland. Geological Magazine, Volume 111, pages 501-504.

Strong, D.F. and Williams, H.
1972: Early Paleozoic flood basalts of northwestern Newfoundland: their petrology and tectonic significance. Geological Association of Canada, Volume 24, pages 43-53.

Sun, S.S. and McDonough, W.F.
1989: Chemical and isotopic systematics of ocean basalts: implications for mantle composition and processes. Geological Society Special Publication 42, pages 313-345.

Tate, M.C. and Clarke, D.B.
1993: Origin of the Late Devonian Weekend lamprophyre dykes, Meguma Zone, Nova Scotia. Canadian Journal of Earth Sciences, Volume 30, pages 2295-2304.

Tuach, J.
1987: Mineralized enviroments, metallogenesis, and the Doucers Valley Fault Complex, eestern White Bay: A philosophy for gold exploration in Newfoundland. *In*

Current Research. Newfoundland Department of Mines and Energy, Mineral Development Division, Report 87-1, pages 129-144.

van Staal, C.R.
2007: Pre-Carboniferous tectonic evolution and metallogeny of the Canadian Appalachians. *In* Mineral Deposits of Canada: A Synthesis of Major Deposit Types, District Metallogeny, the Evoloution of Geological Provinces, and Exploration Methods. *Edited by* W.D. Goodfellow. Geological Association of Canada, Mineral Deposits Division, Special Publication No. 5, pages 783-818.

Whalen, J.B., Currie, K.L. and CHappell, B.W.
1987: A-type granites: geochemical characteristics, discrimination and petrogenesis. Contributions to Mineral Petrology, Volume 95, pages 407-419.

Williams, H.
1976: Tectonic stratigraphic subdivision of the Appalachian Orogen. Geological Society of America, Abstracts with Programs, Volume 8.

1995a: Introduction: Chapter 1. *In* Geology of the Appalachian-Caledonian Orogen in Canada and Greenland. *Edited by* H. Williams. Geological Survey of Canada, Geology of Canada, pages 1-19.

1995b: Temporal and Spatial Divisions; Chapter 2. *In* Geology of the Appalachian-Caledonian Orogen in Canada and Greenland. *Edited by* H. Williams. Geological Survey of Canada, Geology of Canada, pages 21-44.

Williams, H. and Stevens, R.K.
1969: Geology of Belle Isle-Northern extremity of the deformed Appalachian miogeosynclinal belt. Canadian Journal of Earth Sciences, Volume 6, pages 1145-1157.

Winchester, J.A. and Floyd, P.A.
1977: Geochemical discrimination of different magma series and their differentiation products using immobile elements. Chemical Geology, Volume 20, pages 325-343.

Wyman, D.A. and Kerrich, R.
1989: Archean lamprophyre dykes of the Superior Province, Canada: Distribution, petrology, and geochemical characteristics. Journal of Geophysical Research, Volume 94, pages 4667-4696.